

## Interaction of a hydrogenlike ion with a planar topological insulator

A. Martín-Ruiz<sup>1,2,\*</sup> and L. F. Urrutia<sup>1,†</sup>

<sup>1</sup>*Instituto de Ciencias Nucleares, Universidad Nacional Autónoma de México, 04510 México, Distrito Federal, México*

<sup>2</sup>*Instituto de Ciencia de Materiales de Madrid, CSIC, Cantoblanco, 28049 Madrid, Spain*



(Received 18 September 2017; published 7 February 2018)

An electric charge near the surface of a topological insulator (TI) induces an image magnetic monopole. Here we study the spectra of hydrogenlike ions near the surface of a planar TI, taking into account the modifications which arise due to the presence of the image monopole magnetic fields. In fact, the atom-TI interaction provides additional contributions to the Casimir-Polder potential while the ion-TI interaction modifies the energy shifts in the spectrum, which now became distance dependent. We show that the hyperfine structure is sensitive to the image magnetic monopole fields in states with nonzero angular momentum and that circular Rydberg ions can enhance the maximal energy shifts. We discuss in detail the energy splitting of the  $nP_{1/2}$  and  $nP_{3/2}$  states in hydrogen. We also analyze the Casimir-Polder potential and find that this magnetic interaction produces a large-distance repulsive tail for some particular atomic states. A sizable value of the maximum of the potential requires TIs with very low values of the permittivity together with high values of the topological magnetoelectric polarization.

DOI: [10.1103/PhysRevA.97.022502](https://doi.org/10.1103/PhysRevA.97.022502)

### I. INTRODUCTION

Most quantum states of matter are categorized by the symmetries they break, and they are described by effective Landau-Ginzburg theories [1]. However, topological phases evade traditional symmetry-breaking classification schemes. Instead, in the low-energy limit, they are described by topological field theories with quantized coefficients [2]. For instance, the quantum Hall effect is described by the topological Chern-Simons theory in (2+1) dimensions (D) [3], with coefficient corresponding to the quantized Hall conductance. Recently, topological insulators (TIs) in (3+1)D have attracted great attention in condensed matter physics. These materials display nontrivial topological order and are characterized by a fully insulating bulk together with gapless surface states, which are protected by time-reversal (TR) symmetry [4,5]. This type of topological behavior was first predicted in graphene [6]. It was subsequently predicted and then observed in alloys and stoichiometric crystals that display sufficiently strong spin-orbit coupling to induce band inversion, such as  $\text{Bi}_{1-x}\text{Sb}_x$  [7,8],  $\text{Bi}_2\text{Se}_3$ ,  $\text{Bi}_2\text{Te}_3$ ,  $\text{Sb}_2\text{Te}_3$  [9,10], and  $\text{TlBiSe}_2$  [11]. These discoveries stimulate further exploration of the exotic properties of the TIs.

The peculiar properties of TIs stem from a nontrivial topology of their band structure but also interesting properties at the macroscopic level emerge when they interact with, for example, electromagnetic fields [2]. The full theory accounting for the electromagnetic response of TIs is given by the standard Maxwell Lagrangian plus the additional term  $\mathcal{L}_\theta = (\alpha/4\pi^2)\theta\mathbf{E} \cdot \mathbf{B}$ , where  $\mathbf{E}$  and  $\mathbf{B}$  are the electromagnetic fields,  $\alpha$  is the fine structure constant, and  $\theta$  is an angular variable known in particle physics as the axion angle [12]. In

general, the axion angle  $\theta$  is a dynamical field; however, as far as the electromagnetic response of TIs is concerned, it is quantized in odd integer values of  $\pi$ , i.e.,  $\theta = \pm(2n+1)\pi$ , where  $n \in \mathbb{Z}^+$ , and it can be viewed as a phenomenological parameter in the sense of an effective Landau-Ginzburg theory.

One of the most striking features of this topological response theory is the topological magnetoelectric effect (TME), which consists of a mixing between the electric  $\mathbf{E}$  and magnetic induction  $\mathbf{B}$  fields at the surface of the material. This is why, in the condensed matter literature, the axion angle is termed the topological magnetoelectric polarization (TMPE). Among the remarkable consequences of the TME, with which we are concerned here, is the appearance of image magnetic monopoles when a pointlike electric charge is brought near to the surface of a TI. This effect, known as the image magnetic monopole effect, was first derived in Ref. [13] using the usual method of images of electromagnetism; however, it has also been obtained using different methods, e.g., by the action of the  $\text{SL}(2, \mathbb{Z})$  duality group on TIs [14] and by Green's function techniques [15]. The existence of these image magnetic monopoles is compatible with the Maxwell equation  $\nabla \cdot \mathbf{B} = 0$ , since the resulting magnetic fields are in fact induced by circulating vortex Hall currents on the surface of the TI, which are sourced by the electric charge next to the interface rather than by a real pointlike magnetic charge. Other TMEs involving the appearance of image current and charge densities of magnetic monopoles have been predicted [15]. Additional effects due to the TME have been envisioned. For example, when polarized light propagates through a TI surface, of which the surface states has been gapped by TR symmetry breaking, a topological Faraday rotation of 1–10 mrad appears, which falls in a small window but within the current experimental reach [16–21]. On the other hand, the effects of the topological nontriviality on the Casimir effect has also been considered [22–24].

\*alberto.martin@nucleares.unam.mx

†urrutia@nucleares.unam.mx

The experimental determination of the TME arising from TIs in (3+1)D has proved to be rather difficult. This is so because there is an important difference between the  $\theta$  term for (3+1)D topological insulators and the (2+1)D Chern-Simons term for quantum Hall systems [4]. In (2+1)D, a simple dimensional analysis reveals that the topological Chern-Simons term dominates over the nontopological Maxwell term at low energies. However, in (3+1)D, both terms are equally important at low energies since they have the same scaling dimension. This implies that, for (3+1)D TIs, the topological response always coexists with the ordinary electromagnetic response, thus making the detection of the TME of TIs experimentally challenging. Despite this limitation, it was recently reported the measurement of a universal topological Faraday rotation angle equal to the fine structure constant when linearly polarized radiation passes through two surfaces of the TI HgTe [25].

In order to motivate our approach to study the TME, let us recall that the presence of an atom in front of a material body will modify its quantum properties, such as the magnitude of the energy levels and the decay rates of the excited states, which now become functions of the distance between the atom and the body. For a given quantum state, the energy of each atomic level can be interpreted as the interaction energy of the system, yielding the Casimir-Polder (CP) potential experienced by the atom in this state. In this way, distance-dependent energy levels of an atom can be analyzed from two alternative perspectives, which have been very successful and well studied along the years: (i) the investigation of dispersion forces [26,27] and (ii) the consideration of atomic spectroscopy [28]. According to Ref. [26], we will denote by CP interactions those between an atom and a body. In a first approximation, the CP interaction can be understood as arising from the dipole induced by the polarization of the atom, which interacts with an image dipole inside the material required to satisfy the boundary conditions at the surface of the body. If the material body is, for example, a topological insulator, additional interactions arise due to the TME: The charges in the atom will also induce image magnetic monopoles inside the TI, which will in turn interact with the electron via the standard minimal coupling. Since the calculation of the nonretarded force on a charge in front of a metallic plate [29], followed by its generalization including retardation [30], the CP interaction has been profusely studied in diverse materials and geometries. Such extensive interest is motivated by the relevance of CP forces in many branches of science like field theory, cosmology, molecular physics, colloid science, biology, astrophysics, and micro- and nanotechnology, for example. The measurement of CP forces has also experienced a high degree of sophistication ranging from experiments based upon classical scattering [31,32], quantum scattering [33,34], and spectroscopic measurements [32,35,36]. For a detailed account of the theoretical and experimental work on the CP interaction, including the appropriate references, see, for example, Ref. [26].

Within the realm of atomic spectroscopy and because of the well-developed theory together with a large tradition in high-precision measurements, hydrogenlike ions could provide an attractive test bed for studying the TME, since their hyperfine structure turns out to be sensitive to the image monopole magnetic fields. The case of circular Rydberg ions will be of

relevance because they provide an enhancement of the TME contribution with respect to the optical one.

The specific problem we shall consider is that of an hydrogenlike ion, including the case of a hydrogen atom, near the surface of a TI. The TI is assumed to be covered with a thin magnetic layer to gap the surface states. Because of the TME, the atomic charges produce image magnetic monopoles inside the TI, whose magnetic fields cause additional small shifts in the energy levels of the ion. For a given state, the corresponding energy provides the nonretarded CP potential as well as the distance-dependent energy shifts. Also, we discuss the spectra of the lines where the contributions from the TME induced by the topological insulator arise. Since the splitting of the energy levels depends mainly on the ion-surface distance, we focus on the case where (i) there is a negligible wave-function overlap between the electron and the surface states, (ii) the ion-TI interaction is dominated by nonretarded electromagnetic forces, and (iii) perturbation theory is valid.

The paper is organized as follows. In Sec. II, we review the basics of the electromagnetic response of TR-invariant topological insulators in (3+1)D. The Hamiltonian describing the interaction of the ion with the TI is derived in Sec. III. We analyze the order of magnitude of each contribution and we retain the more important ones. The energy shifts of circular Rydberg hydrogenlike ions are discussed in Sec. IV, where we consider the separate cases where the ion and the TI are embedded either in the same dielectric media or in a different one. The former situation also contributes to the amplification of the TME. Section V includes the calculation of the energy level shifts of the hyperfine spectrum of the hydrogen in the  $nP_{3/2}$  and  $nP_{1/2}$  states, which constitute the basis for the analysis in the next section, Sec. VI, where we discuss the resulting Casimir-Polder interaction in each of the previously determined states. A concluding summary of our results and a discussion on the limitations of our model constitutes Sec. VII. Throughout the paper, Lorentz-Heaviside units are assumed ( $\hbar = c = 1$ ) and the metric signature will be taken as  $(+, -, -, -)$  and  $\epsilon^{0123} = +1$ .

## II. ELECTROMAGNETIC RESPONSE OF (3+1)D TOPOLOGICAL INSULATORS

The low-energy effective field theory governing the electromagnetic response of (3+1)D topological insulators, independently of the microscopic details, is defined by the action

$$S = \int \left[ \frac{1}{8\pi} \left( \epsilon \mathbf{E}^2 - \frac{1}{\mu} \mathbf{B}^2 \right) + \frac{\alpha}{4\pi^2} \theta \mathbf{E} \cdot \mathbf{B} \right] d^4x, \quad (1)$$

where  $\mathbf{E}$  and  $\mathbf{B}$  are the electromagnetic fields,  $\alpha \simeq 1/137$  is the fine structure constant,  $\epsilon$  and  $\mu$  are the permittivity and permeability, respectively, and  $\theta$  is the TMEP (axion field). When the theory is defined on a manifold without boundary, TR symmetry indicates that there are only two nonequivalent allowed values of  $\theta$ , which are 0 and  $\pi$  modulo  $2\pi$ . This leads to the  $\mathbb{Z}_2$  classification of three-dimensional TR-invariant TIs. For a manifold with a boundary, TR symmetry is broken even if  $\theta = \pi$  (modulo  $2\pi$ ) in the action (1), and nontrivial metallic surface states appear. The theory is a fair description of the whole system (bulk + boundary) only when a TR-breaking

perturbation is induced on the surface to gap the surface states, for instance, by means of a magnetic perturbation (applied field and/or film coating) [4,5] or even by using commensurate out- and in-plane antiferromagnetic or ferrimagnetic insulating thin films [37]. These surface states have an anomaly which cancels the TR-breaking term, thus restoring the TR symmetry of the whole system. In this situation,  $\theta$  is quantized in odd integer values of  $\pi$  such that  $\theta = \pm(2n + 1)\pi$ , where  $2n + 1$  corresponds to the number of Dirac fermions on the surface. In this work, we consider that the TR perturbation is a magnetic coating of small thickness, such that the two signs correspond to the two possible orientations of the magnetization in the direction perpendicular to the surface. Physically, the axionic term in Eq. (1) is generated by a quantized Hall effect on the surface of the TI leading to a quantized magnetoelectric response in units of the fine structure constant.

The electromagnetic response of TIs is still described by the ordinary Maxwell equations

$$\begin{aligned}
 \nabla \cdot \mathbf{D} &= 4\pi\rho, & \nabla \times \mathbf{H} &= \frac{\partial \mathbf{D}}{\partial t} + 4\pi\mathbf{J}, \\
 \nabla \cdot \mathbf{B} &= 0, & \nabla \times \mathbf{E} &= -\frac{\partial \mathbf{B}}{\partial t},
 \end{aligned} \quad (2)$$

with the modified constitutive relations

$$\mathbf{D} = \varepsilon\mathbf{E} + \frac{\alpha}{\pi}\theta\mathbf{B}, \quad \mathbf{H} = \frac{1}{\mu}\mathbf{B} - \frac{\alpha}{\pi}\theta\mathbf{E}. \quad (3)$$

The first term in each constitutive relation is the usual electromagnetic term defined in terms of the permittivity and permeability functions, giving rise to the ordinary electromagnetic phenomena. Interestingly, the second term in each constitutive relation, which arises from the axionic term in Eq. (1), leads to a mixing between the electric  $\mathbf{E}$  and magnetic induction  $\mathbf{B}$  fields. Importantly, the quantization of the TMEP depends only on the TR symmetry and the bulk topology; it is therefore universal and independent of any material details, thus guaranteeing the robustness of the TME.

The general solution to the modified Maxwell equations (2) in the presence of planar, spherical, and cylindrical TIs has been recently elaborated by means of Green's function techniques [15,38,39]. Knowledge of the Green's function allows one to compute the electromagnetic potential  $A^\mu = (\phi, \mathbf{A})$  at any point from an arbitrary distribution of sources  $J^\mu = (\rho, \mathbf{J})$  via

$$A^\mu(\mathbf{r}) = \int G^\mu_\nu(\mathbf{r}, \mathbf{r}') J^\nu(\mathbf{r}') d^3\mathbf{r}', \quad (4)$$

where the Green's function  $G^\mu_\nu$  contains all the information concerning the geometry and boundary conditions on the surface of the TI. Because of the gauge invariance of the action (1), the electrostatic and magnetostatic fields are defined in terms of the potential  $A^\mu$  according to  $\mathbf{E} = -\nabla\phi$  and  $\mathbf{B} = \nabla \times \mathbf{A}$ , as usual. As can be seen from Eq. (4), the nondiagonal components of the Green's function are the responsibility of the TME.

### III. HYDROGENLIKE ION NEAR THE SURFACE OF A TI

Let us consider an hydrogenlike ion near a three-dimensional TI half-space, as shown in Fig. 1, and let us restrict ourselves to the nonretarded approximation. As is well known,

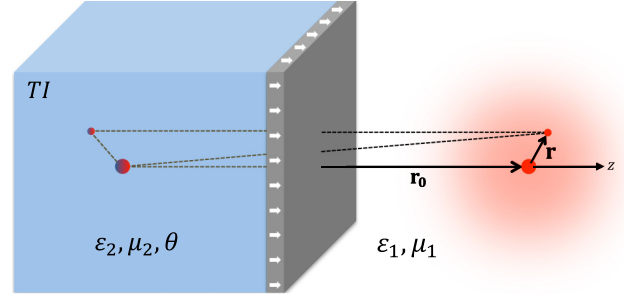


FIG. 1. An hydrogenlike ion at position  $\mathbf{r}_0$  near a three-dimensional TI. The TI is covered with a thin magnetic layer of thickness  $w \ll |\mathbf{r}_0|$  (not to scale) which controls the sign of the TMEP  $\theta$ .

this regime is valid for distances  $b$  such that  $b \ll \lambda_C$ , where  $\lambda_C$  can be estimated as the maximum wavelength characterizing the transitions between the specific energy levels being probed in the ion [26,40]. In what follows we will consider the nucleus to be fixed at  $\mathbf{r}_0 = b\hat{\mathbf{e}}_z$ , and we assume that the TI is covered with a thin magnetic layer of thickness  $w \ll b$  and magnetization  $\mathbf{M} = M\hat{\mathbf{e}}_z$ , such that there is a negligible wave-function overlap between the atomic electron and the surface states. Thus, we henceforth assume that  $w \ll b \ll \lambda_C$ . We stress here that the only effect of the magnetic coating is to gap the surface states. However, the ferromagnet makes a magnetic field and the energy shifts of the atomic spectrum are to be measured as a function of the magnetization  $M$ . The effects we shall discuss in the following are defined as the linear extrapolation of the energy shifts as  $M \rightarrow 0^+$ , in which limit the nontopological contributions are removed. In Sec. VII, we will discuss the effects of the magnetic coating on the energy levels in more detail.

In the nonretarded regime, the CP interaction between two atoms (two hydrogen atoms, for instance) is achieved by computing the Coulomb interaction between all charges of one atom and all charges of the other. Since in our model we have to take into account many pairwise Coulomb interactions (between the charges of the atom and their electric images), it is convenient to introduce the Coulomb interaction Hamiltonian,

$$U_{\text{Coul}} = \frac{1}{2} \int \rho(\mathbf{r}) G^0_0(\mathbf{r}, \mathbf{r}') \rho(\mathbf{r}') d^3\mathbf{r} d^3\mathbf{r}', \quad (5)$$

where  $\rho$  includes the two opposite charges of the ion.

Because of the TME, the atomic charges will also produce image magnetic monopoles located inside the TI, whose magnetic fields will in turn interact with the atomic electron. This interaction results from the coupling of the magnetic field produced by the image monopoles with the electron spin and their orbital motion. Therefore, the Hamiltonian we consider is

$$H = \frac{\mathbf{\Pi}^2}{2m_e} + U_{\text{Coul}} + \frac{e}{m_e} \mathbf{S} \cdot \mathbf{B} + V_{\text{fs}} + V_{\text{hfs}}, \quad (6)$$

where  $m_e$  is the electron mass,  $e > 0$  is the magnitude of the electron charge,  $\mathbf{\Pi} = \mathbf{p} + e\mathbf{A}$  is the canonical momentum, and  $\mathbf{B} = \nabla \times \mathbf{A}$  is the magnetic field associated with the image magnetic monopoles, one contribution arising from the nucleus and the other from the electron. Besides,  $U_{\text{Coul}}$  is the Coulomb

interaction energy (5),  $V_{fs}$  are the fine structure contributions (relativistic energy correction, spin-orbit coupling, and Darwin term), and  $V_{hfs}$  is the hyperfine interaction.

In our Hamiltonian, we have considered those terms which give the most important contributions to the energy spectrum. However, there are other smaller terms, such as the interaction between the image monopole magnetic fields and the nuclear spin, and also the interaction between the image electric dipole produced by the atomic magnetic moment and the atomic electric dipole. Next let us study each term separately.

Since the ion-surface distance, though small to make retardation effects negligible, is much greater than the Bohr radius  $a_0$ , a Taylor expansion in the electromagnetic fields can be performed [40–42]. Then, treating the ion as an electric composite system, the effective charge density can be written as

$$\rho(\mathbf{r}') = e[Z\delta(\mathbf{r}' - \mathbf{r}_0) - \delta(\mathbf{r}' - \mathbf{r}_0 - \mathbf{r})], \quad (7)$$

where  $Z$  is the atomic number and  $\mathbf{r}$  is the vector which localizes the electron from the nucleus. It is convenient to split the 00 component of the Green's function as [15]

$$G_0^0(\mathbf{r}, \mathbf{r}') = G(\mathbf{r}, \mathbf{r}') + G_S(\mathbf{r}, \mathbf{r}'), \quad (8)$$

where the first term

$$G(\mathbf{r}, \mathbf{r}') = \frac{1}{\sqrt{(x-x')^2 + (y-y')^2 + (z-z')^2}} \quad (9)$$

is the Green's function in unbounded space. The second term

$$G_S(\mathbf{r}, \mathbf{r}') = \frac{\kappa}{\sqrt{(x-x')^2 + (y-y')^2 + (z+z')^2}}, \quad (10)$$

with

$$\kappa = \frac{1}{\varepsilon_1} \frac{(\varepsilon_1 - \varepsilon_2)(1/\mu_1 + 1/\mu_2) - \tilde{\theta}^2}{(\varepsilon_1 + \varepsilon_2)(1/\mu_1 + 1/\mu_2) + \tilde{\theta}^2}, \quad \tilde{\theta} \equiv \alpha \frac{\theta}{\pi}, \quad (11)$$

is a solution of the homogeneous Laplace equation, such that  $G_0^0(\mathbf{r}, \mathbf{r}')$  satisfies the required boundary conditions at the surface of the TI [22]. Let us emphasize that  $\tilde{\theta}$  in Eq. (11) is of order  $\alpha$ . Using the aforementioned charge distribution and the Green's functions, the Coulomb interaction (5) becomes

$$\begin{aligned} U_{\text{Coul}} = & \frac{e^2}{2} [Z^2 G(\mathbf{r}_0, \mathbf{r}_0) - 2ZG(\mathbf{r}_0 + \mathbf{r}, \mathbf{r}_0) \\ & + G(\mathbf{r}_0 + \mathbf{r}, \mathbf{r}_0 + \mathbf{r})] \\ & + \frac{e^2}{2} [Z^2 G_S(\mathbf{r}_0, \mathbf{r}_0) + G_S(\mathbf{r}_0 + \mathbf{r}, \mathbf{r}_0 + \mathbf{r}) \\ & - ZG_S(\mathbf{r}_0, \mathbf{r}_0 + \mathbf{r}) - ZG_S(\mathbf{r}_0 + \mathbf{r}, \mathbf{r}_0)]. \quad (12) \end{aligned}$$

The terms  $Z^2 G(\mathbf{r}_0, \mathbf{r}_0)$  and  $G(\mathbf{r}_0 + \mathbf{r}, \mathbf{r}_0 + \mathbf{r})$  in this expression are the divergent self-energies of the nucleus and the electron, respectively, which we discard. The term  $ZG(\mathbf{r}_0, \mathbf{r}_0 + \mathbf{r})$  corresponds to the nucleus-electron interaction. The contributions due to the presence of the TI are given by the remaining four terms and the Coulomb energy now takes the form

$$\begin{aligned} U_{\text{Coul}} = & -\frac{Ze^2}{\varepsilon_1 r} + \frac{e^2}{2} [Z^2 G_S(\mathbf{r}_0, \mathbf{r}_0) - ZG_S(\mathbf{r}_0 + \mathbf{r}, \mathbf{r}_0) \\ & - ZG_S(\mathbf{r}_0, \mathbf{r}_0 + \mathbf{r}) + G_S(\mathbf{r}_0 + \mathbf{r}, \mathbf{r}_0 + \mathbf{r})]. \quad (13) \end{aligned}$$

In the limit  $|\mathbf{r}| \ll |\mathbf{r}_0|$ , when the dimensions of the ion are small compared with the nucleus-interface distance  $|\mathbf{r}_0|$ , the additional terms can be written as derivatives of  $G_S$ . Making a Taylor expansion of  $G_S(\mathbf{r}_0, \mathbf{r}_0 + \mathbf{r})$  in powers of  $\mathbf{r}$  up to second order produces

$$\begin{aligned} G_S^{(2)}(\mathbf{r}_0, \mathbf{r}_0 + \mathbf{r}) \simeq & G_S(\mathbf{r}_0, \mathbf{r}_0) + (\mathbf{r} \cdot \nabla') G_S(\mathbf{r}_0, \mathbf{r}')|_{\mathbf{r}'=\mathbf{r}_0} \\ & + \frac{1}{2} (\mathbf{r} \cdot \nabla')^2 G_S(\mathbf{r}_0, \mathbf{r}')|_{\mathbf{r}'=\mathbf{r}_0}. \quad (14) \end{aligned}$$

Analogously, a Taylor expansion for  $G_S(\mathbf{r}_0 + \mathbf{r}, \mathbf{r}_0)$  yields

$$\begin{aligned} G_S^{(2)}(\mathbf{r}_0 + \mathbf{r}, \mathbf{r}_0) \simeq & G_S(\mathbf{r}_0, \mathbf{r}_0) + (\mathbf{r} \cdot \nabla') G_S(\mathbf{r}', \mathbf{r}_0)|_{\mathbf{r}'=\mathbf{r}_0} \\ & + \frac{1}{2} (\mathbf{r} \cdot \nabla')^2 G_S(\mathbf{r}', \mathbf{r}_0)|_{\mathbf{r}'=\mathbf{r}_0}. \quad (15) \end{aligned}$$

Using the previous results, one can further establish

$$\begin{aligned} G_S^{(2)}(\mathbf{r}_0 + \mathbf{r}, \mathbf{r}_0 + \mathbf{r}) + G_S(\mathbf{r}_0, \mathbf{r}_0) \\ \simeq & G_S^{(2)}(\mathbf{r}_0, \mathbf{r}_0 + \mathbf{r}) + G_S^{(2)}(\mathbf{r}_0 + \mathbf{r}, \mathbf{r}_0) \\ & + (\mathbf{r} \cdot \nabla')(\mathbf{r} \cdot \nabla'') G_S(\mathbf{r}', \mathbf{r}'')|_{\mathbf{r}'=\mathbf{r}''=\mathbf{r}_0}. \quad (16) \end{aligned}$$

Substituting the expressions (14), (15), and (16) in Eq. (13) yields our final expression for the Coulomb energy

$$\begin{aligned} U_{\text{Coul}} = & -\frac{Ze^2}{\varepsilon_1 r} + \frac{(Z-1)^2 e^2}{2} G_S(\mathbf{r}_0, \mathbf{r}_0) \\ & + (1-Z)e^2 \left[ (\mathbf{r} \cdot \nabla') G_S(\mathbf{r}_0, \mathbf{r}') \Big|_{\mathbf{r}'=\mathbf{r}_0} \right. \\ & \left. + \frac{1}{2} (\mathbf{r} \cdot \nabla')^2 G_S(\mathbf{r}_0, \mathbf{r}') \Big|_{\mathbf{r}'=\mathbf{r}_0} \right] \\ & + \frac{e^2}{2} (\mathbf{r} \cdot \nabla')(\mathbf{r} \cdot \nabla'') G_S(\mathbf{r}', \mathbf{r}'') \Big|_{\mathbf{r}'=\mathbf{r}''=\mathbf{r}_0}. \quad (17) \end{aligned}$$

Using the Green's function  $G_S$  defined above, one obtains

$$\begin{aligned} G_S(\mathbf{r}_0, \mathbf{r}_0) = & \frac{\kappa}{2b}, \quad (\mathbf{r} \cdot \nabla'') G_S(\mathbf{r}_0, \mathbf{r}'')|_{\mathbf{r}''=\mathbf{r}_0} = -\frac{\kappa z}{4b^2}, \\ (\mathbf{r} \cdot \nabla')(\mathbf{r} \cdot \nabla') G_S(\mathbf{r}', \mathbf{r}_0)|_{\mathbf{r}'=\mathbf{r}_0} = & \kappa \frac{3z^2 - r^2}{8b^3}, \\ (\mathbf{r} \cdot \nabla')(\mathbf{r} \cdot \nabla'') G_S(\mathbf{r}', \mathbf{r}'')|_{\mathbf{r}'=\mathbf{r}''=\mathbf{r}_0} = & \kappa \frac{r^2 + z^2}{8b^3}, \quad (18) \end{aligned}$$

such that the Coulomb interaction simplifies to

$$U_{\text{Coul}} = -\frac{Ze^2}{\varepsilon_1 r} + \delta U_0 + \delta U_1 + \delta U_2. \quad (19)$$

The first term is the usual Coulomb interaction experienced by the atomic electron due to the nucleus. The second term,  $\delta U_0 = \kappa(Z-1)^2(e^2/4b)$ , which corresponds to the interaction between the effective atomic charge and its own image, does not depend on the electron coordinates and thus it is not considered for the purposes of this paper. The last terms,

$$\delta U_1 = \frac{\kappa(Z-1)e^2}{4b^2} z, \quad \delta U_2 = \frac{\kappa e^2}{16b^3} [Zr^2 - (3Z-4)z^2], \quad (20)$$

constitute the optical contribution to the attractive CP interaction due to the presence of the TI.



Now let us consider the terms which are the direct manifestation of the image monopole magnetic fields, i.e.,  $(e/m_e)\mathbf{A} \cdot \mathbf{p}$  and  $(e^2/2m_e)\mathbf{A}^2$ . These terms will provide additional corrections to the standard CP interaction arising from the presence of the TI. In terms of the Green's function  $G^i_0(\mathbf{x}, \mathbf{x}')$  [15], the vector potential is

$$A^i(\mathbf{x}) = \int G^i_0(\mathbf{x}, \mathbf{x}') \rho(\mathbf{x}') d^3\mathbf{x}', \quad (21)$$

where  $\rho$  is the previously defined charge density in Eq. (7). This yields

$$A^i(\mathbf{x}) = ZeG^i_0(\mathbf{x}, \mathbf{r}_0) - eG^i_0(\mathbf{x}, \mathbf{r}_0 + \mathbf{r}). \quad (22)$$

In the coordinate system attached to the nucleus, the vector potential becomes

$$A^i(\mathbf{r}) = ZeG^i_0(\mathbf{r}_0 + \mathbf{r}, \mathbf{r}_0) - eG^i_0(\mathbf{r}_0 + \mathbf{r}, \mathbf{r}_0 + \mathbf{r}). \quad (23)$$

The first term corresponds to the vector potential produced by the image monopole of the nucleus on the electron, while the second term is the vector potential of the image monopole of the electron on the electron itself. The calculation of the vector potential (23) starts from the components of the Green's function

$$eG^i_0(\mathbf{x}, \mathbf{x}') = \frac{g\epsilon^{0ji3}R_j}{R^2} \left( 1 - \frac{z+z'}{\sqrt{R^2+(z+z')^2}} \right), \quad (24)$$

where  $R^j = (x-x')\hat{\mathbf{e}}_x + (y-y')\hat{\mathbf{e}}_y$  and

$$g = \frac{2e\tilde{\theta}}{(\epsilon_1 + \epsilon_2)(1/\mu_1 + 1/\mu_2) + \tilde{\theta}^2} \quad (25)$$

is the magnitude of the image magnetic monopole of an electric charge  $e$ . From Eq. (24), we observe that the expression  $G^i_0(\mathbf{x}, \mathbf{x})$  is ill defined at a first glance. This calls for a careful determination of the limit  $\mathbf{x} \rightarrow \mathbf{x}'$ . A Taylor expansion of the term in round brackets in the right-hand side of Eq. (24) leads to

$$eG^i_0(\mathbf{x}, \mathbf{x}') \simeq \frac{g\epsilon^{0ji3}R_j}{2} \left[ \frac{1}{(z+z')^2} + O\left(\frac{R^{2(n-1)}}{(z+z')^{2n}}\right) \right]. \quad (26)$$

Taking the limit  $\mathbf{x}' \rightarrow \mathbf{x}$ , we obtain that  $R_j \rightarrow 0$  and  $z+z' = 2z$ , in such a way that  $G^i_0(\mathbf{x}, \mathbf{x}) = 0$ . Then, Eq. (23) reduces to

$$A^i(\mathbf{r}) = ZeG^i_0(\mathbf{r}_0 + \mathbf{r}, \mathbf{r}_0). \quad (27)$$

Since  $|\mathbf{r}| \ll |\mathbf{r}_0|$ , we perform a Taylor expansion up to third order in  $\mathbf{r}$  to obtain

$$\begin{aligned} A^i(\mathbf{r}) \simeq & Ze \left[ G^i_0(\mathbf{r}_0, \mathbf{r}_0) + (\mathbf{r} \cdot \nabla') G^i_0(\mathbf{x}', \mathbf{r}_0) \right. \\ & + \frac{1}{2!} (\mathbf{r} \cdot \nabla')^2 G^i_0(\mathbf{x}', \mathbf{r}_0) \\ & \left. + \frac{1}{3!} (\mathbf{r} \cdot \nabla')^3 G^i_0(\mathbf{x}', \mathbf{r}_0) \right] \Big|_{\mathbf{x}'=\mathbf{r}_0}. \end{aligned} \quad (28)$$

The first term in the right-hand side of the above equation is zero and the subsequent contributions require also an accurate

calculation of the corresponding limit. Using the Green's function  $G^i_0$  defined above, one obtains

$$\begin{aligned} (\mathbf{r} \cdot \nabla') G^i_0(\mathbf{x}', \mathbf{r}_0) \Big|_{\mathbf{x}'=\mathbf{r}_0} &= -\frac{g}{8b^2} \epsilon^{0ij3} r_j, \\ (\mathbf{r} \cdot \nabla')^2 G^i_0(\mathbf{x}', \mathbf{r}_0) \Big|_{\mathbf{x}'=\mathbf{r}_0} &= \frac{gz}{4b^3} \epsilon^{0ij3} r_j, \\ (\mathbf{r} \cdot \nabla')^3 G^i_0(\mathbf{x}', \mathbf{r}_0) \Big|_{\mathbf{x}'=\mathbf{r}_0} &= \frac{9g}{64b^4} (r^2 - 5z^2) \epsilon^{0ij3} r_j. \end{aligned} \quad (29)$$

In this way, the final expression for the vector potential is

$$A^i(\mathbf{r}) = -\frac{Zge}{8b^2} \left( 1 - \frac{z}{b} - \frac{3}{16} \frac{r^2 - 5z^2}{b^2} \right) \epsilon^{0ij3} r_j. \quad (30)$$

The final contribution of the term  $\mathbf{A} \cdot \mathbf{p}$  to the Hamiltonian is

$$\frac{e}{m_e} \mathbf{A} \cdot \mathbf{p} = \delta V_{\theta 1} + \delta V_{\theta 2} + \delta V_{\theta 3}, \quad (31)$$

with

$$\begin{aligned} \delta V_{\theta 1} &= -\frac{Zge}{8m_e b^2} L_z, \quad \delta V_{\theta 2} = -\frac{z}{b} \delta V_{\theta 1}, \\ \delta V_{\theta 3} &= -\frac{3}{16} \frac{r^2 - 5z^2}{b^2} \delta V_{\theta 1}, \end{aligned} \quad (32)$$

where  $L_z = xp_y - yp_x$  is the  $z$  component of the angular momentum operator.

Next we deal with the quadratic term in the vector potential appearing in the Hamiltonian (6). As shown in the expression (20) for the contribution  $\delta U$ , we are considering corrections up the quadratic order in the electron coordinates. Using the corresponding vector potential (30), we thus find

$$\frac{e^2}{2m_e} \mathbf{A}^2 = \frac{(Zge)^2}{128m_e b^4} (r^2 - z^2). \quad (33)$$

A similar analysis is next performed for the magnetic interaction  $(e/m_e)\mathbf{S} \cdot \mathbf{B}$ , where the magnetic field  $\mathbf{B}$  is produced by the image monopoles of the nucleus and the electron. The nucleus is located at  $\mathbf{r}_0 = b\hat{\mathbf{e}}_z$  and produces an image monopole of magnitude  $Zg$  at  $-\mathbf{r}_0$ . In our coordinate system, the magnetic field of such image monopole acting on the electron is

$$\mathbf{B}_n = Zg \frac{\mathbf{r} + 2\mathbf{r}_0}{|\mathbf{r} + 2\mathbf{r}_0|^3} = Zg \frac{x\hat{\mathbf{e}}_x + y\hat{\mathbf{e}}_y + (z+2b)\hat{\mathbf{e}}_z}{[R^2 + (z+2b)^2]^{3/2}}. \quad (34)$$

The other contribution to the image monopole magnetic field comes from the electron itself and it is located at  $\mathbf{r}' = x\hat{\mathbf{e}}_x + y\hat{\mathbf{e}}_y - (z+b)\hat{\mathbf{e}}_z$  with magnitude  $-g$ . It is given by

$$\mathbf{B}_e = -g \frac{\hat{\mathbf{e}}_z}{4(z+b)^2}. \quad (35)$$

The total magnetic field that feels the electron is then

$$\mathbf{B} = Zg \frac{x\hat{\mathbf{e}}_x + y\hat{\mathbf{e}}_y + (z+2b)\hat{\mathbf{e}}_z}{[R^2 + (z+2b)^2]^{3/2}} - g \frac{\hat{\mathbf{e}}_z}{4(z+b)^2}. \quad (36)$$

Performing a Taylor expansion up to quadratic order in  $\mathbf{r}$ , the magnetic interaction thus takes the final form

$$\frac{e}{m_e} \mathbf{S} \cdot \mathbf{B} = \delta W_{\theta 1} + \delta W_{\theta 2}, \quad (37)$$

where

$$\begin{aligned}\delta W_{\theta 1} &= \frac{ge}{4m_e b^2}(Z-1)S_z, \\ \delta W_{\theta 2} &= \frac{ge}{4m_e b^3} \left[ \frac{Z}{2}(xS_x + yS_y) - (Z-2)zS_z \right].\end{aligned}\quad (38)$$

Having taken into account each of the previous contributions to their lowest order in  $x_i/b^2$ , the Hamiltonian (6) reduces to

$$\begin{aligned}H &= H_0 + \frac{\kappa(Z-1)e^2}{4b^2}z + \frac{\kappa e^2}{16b^3}[Zr^2 - (3Z-4)z^2] \\ &\quad - \frac{Zge}{8m_e b^2} \left( 1 - \frac{z}{b} - \frac{3}{16} \frac{r^2 - 5z^2}{b^2} \right) \mathbf{L}_z \\ &\quad + \frac{(Zge)^2}{128m_e b^4}(r^2 - z^2) + \frac{Zge}{8m_e b^3}(xS_x + yS_y) \\ &\quad + \frac{ge}{4m_e b^2} \left[ (Z-1) - (Z-2)\frac{z}{b} \right] S_z,\end{aligned}\quad (39)$$

where

$$H_0 = \frac{\mathbf{p}^2}{2m_e} - \frac{Ze^2}{\varepsilon_1 r} + H_{\text{fs}} + H_{\text{hfs}}\quad (40)$$

is the Hamiltonian of the hydrogenlike ion including fine ( $H_{\text{fs}}$ ) and hyperfine ( $H_{\text{hfs}}$ ) corrections.

Our next step is to have an estimation of the relative weights of the different contributions to the mean value of the Hamiltonian (39). The exact mean values for a given specific atomic levels will be presented in the next sections. The contributions to the CP potential of the optical terms in the right-hand side (rhs) of Eq. (39) can be estimated as

$$\frac{\langle \delta U_1 \rangle}{E_g} = -\frac{\kappa \varepsilon_1}{2} \frac{Z-1}{Z} \xi^2 \langle \cos \vartheta \rangle,\quad (41)$$

$$\frac{\langle \delta U_2 \rangle}{E_g} = -\frac{\kappa}{8} \left( \frac{\varepsilon_1}{Z} \right)^2 \xi^3 [Z - (3Z-4)\langle \cos^2 \vartheta \rangle],\quad (42)$$

where  $\xi = a_0/b \ll 1$  and  $E_g = -m_e \alpha^2/2 = -13.6\text{eV}$  is the ground-state energy of the hydrogen atom. For  $b$  of the order of  $\mu\text{m}$ , we find  $\xi \sim \alpha^2 \approx 10^{-5}$ , and therefore we expect  $\langle \delta U_1 \rangle \sim 2\kappa \varepsilon_1 \times 10^{-8}\text{eV}$  for  $Z \neq 1$ , and a null value for  $Z = 1$ . In a similar fashion, we expect  $\langle \delta U_2 \rangle \sim 2\kappa(\varepsilon_1/Z)^2 \times 10^{-12}\text{eV}$ . We observe that although these contributions depend crucially on the values of  $\kappa$ ,  $\varepsilon_1$ , and  $Z$ , they are smaller than the hyperfine structure of the hydrogenlike ion  $E_{\text{hfs}} \sim (Z/n\varepsilon_1)^3 \times 10^{-7}\text{eV}$  and for this reason we take  $H_0$  in Eq. (40) as our unperturbed system.

The next term in Eq. (39) arises from the interaction  $(e/m_e)\mathbf{A} \cdot \mathbf{p}$ . A direct estimation shows that only the first term in the rhs of Eq. (31), which is of the order of

$$\frac{\langle \delta V_{\theta 1} \rangle}{E_g} = \frac{Z}{2} \alpha^2 \xi^2 \frac{(\theta/\pi)\langle L_z \rangle}{(\varepsilon_1 + \varepsilon_2)(1/\mu_1 + 1/\mu_2) + \tilde{\theta}^2},\quad (43)$$

can compete with the optical contributions  $\delta U_1$  and  $\delta U_2$ . For  $b \sim \mu\text{m}$ , one finds  $\langle \delta V_{\theta 1} \rangle \sim Z \times 10^{-12}\text{eV}$ , while the other terms are of the order of  $\langle \delta V_{\theta 2} \rangle \sim 5\varepsilon_1 \times 10^{-17}\text{eV}$  and  $\langle \delta V_{\theta 3} \rangle \sim (3\varepsilon_1^2/Z) \times 10^{-21}\text{eV}$ , which are strongly suppressed with respect to  $\langle \delta V_{\theta 1} \rangle$ . Therefore, in the subsequent analysis we only consider the term  $\delta V_{\theta 1}$  while disregarding the others. An interesting feature of this term is that the product  $\theta\langle L_z \rangle$

can be positive or negative, depending on both the sign of the magnetization on the surface of the TI and the projection of the  $z$  component of the angular momentum. When negative, this term provides a positive contribution for the Hamiltonian, thus in principle competing with the attractive character of the CP interaction optical contributions in the CP potential. We make a detailed discussion of this possibility in Sec. VI. This property is a direct consequence of the TME effect.

The next term to be considered is  $(e^2/2m_e)\mathbf{A}^2$ , leading to corrections of the order of

$$\frac{\langle (e^2/2m_e)\mathbf{A}^2 \rangle}{E_g} = -\left[ \frac{\alpha^2 \xi^2 (\theta/\pi)(\varepsilon_1/4)}{(\varepsilon_1 + \varepsilon_2)(1/\mu_1 + 1/\mu_2) + \tilde{\theta}^2} \right]^2.\quad (44)$$

Since  $\xi \sim \alpha^2$  for  $b \sim \mu\text{m}$ , this term is  $\alpha^6 \sim 10^{-13}$  smaller than the optical contributions and will not be taken into account. Finally we are left with the spin-dependent interaction terms in Eq. (39), arising from the interaction proportional to  $\mathbf{S} \cdot \mathbf{B}$ . The most important contribution is

$$\frac{\langle \delta W_{\theta 1} \rangle}{E_g} = \alpha^2 \xi^2 \frac{(1-Z)(\theta/\pi)\langle S_z \rangle}{(\varepsilon_1 + \varepsilon_2)(1/\mu_1 + 1/\mu_2) + \tilde{\theta}^2},\quad (45)$$

which is of the same order of magnitude than  $\langle \delta U_2 \rangle$  and  $\langle \delta V_{\theta 1} \rangle$  for  $b \sim \mu\text{m}$  and  $Z \neq 1$ , and vanishes for the hydrogen atom. Therefore, we retain such term in our subsequent analysis. Note that in an analogous fashion to that of the term  $\delta V_{\theta 1}$ , the sign of this term can be tuned by means of the product  $\theta\langle S_z \rangle$ , which can be either positive or negative depending on both the sign of the magnetization on the surface of the TI and  $z$  component of the spin. One can further verify that the second term,  $\langle \delta W_{\theta 2} \rangle$ , is smaller than  $\langle \delta W_{\theta 1} \rangle$  by a factor of  $\alpha^2 \approx 10^{-5}$ , and thus it can be discarded.

Finally, we make a rough estimation of the weights of the terms not considered in our Hamiltonian (6). We first consider the interaction between the image monopole magnetic fields (36) and the nuclear magnetic moment  $\boldsymbol{\mu} = (Zeg_N/2m_N)\mathbf{I}$ , where  $\mathbf{I}$  is the nuclear spin,  $m_N$  is its mass and  $g_N$  is its gyromagnetic ratio. This is given by  $\delta Q = -\boldsymbol{\mu} \cdot \mathbf{B}$ . Performing a Taylor expansion of the magnetic field, we find similar expressions to those of Eq. (38). Thus we find that the ratio between the most important contributions,  $\delta Q_1 = Z(1-Z)(egg_N/8m_N b^2)L_z$  and  $\delta W_{\theta 1}$ , become

$$\frac{\langle \delta Q_1 \rangle}{\langle \delta W_{\theta 1} \rangle} = \frac{Zg_N}{2} \frac{m_e}{m_N}.\quad (46)$$

As discussed in the previous paragraphs,  $\delta W_{\theta 1}$  is of the order of  $10^{-12}\text{eV}$ , and thus any smaller contribution can be disregarded in our analysis. Indeed, one can directly verify that the ratio (46) is very small ( $\sim 10^{-4}$ ) and this is why we have not considered the  $\delta Q$  interaction in our initial Hamiltonian (6). On the other hand, the magnetic moment of the nucleus  $\boldsymbol{\mu}$  will induce an image electric dipole  $\mathbf{d}$  due to the TME, whose electric field  $\mathbf{E}$  will in turn interact with the atomic dipole moment  $\mathbf{p}$  according to  $\delta P = -\mathbf{p} \cdot \mathbf{E}$ . In this case, the full expression is rather complicated but a rough estimation can be done. We can naively think that the magnetic dipole moment is sourced by an elementary electric current  $\mathbf{j}$  whose magnitude must be proportional to  $|\boldsymbol{\mu}|$ . This implies that the interaction  $\delta P$  must be proportional to  $|\boldsymbol{\mu}|$  (from the source) and to  $g$  (from the nondiagonal components of the Green's function). These

simple arguments imply that  $\langle \delta P \rangle / \langle \delta V_{\theta 1} \rangle \approx (g_N/2)(m_e/m_N)$ , which is small enough to be considered in our analyses.

The previous order of magnitude estimations leave us with

$$H = H_0 + \delta U_1 + \delta U_2 + \delta V_{\theta 1} + \delta W_{\theta 1}, \quad (47)$$

as the final Hamiltonian describing the ion-TI interaction, to be considered in the next sections. Here, each term is given by

$$\delta U_1 = \frac{\varepsilon_1}{2} \frac{1-Z}{Z} \kappa \xi^2 E_g \tilde{z}, \quad (48)$$

$$\delta U_2 = -\frac{\varepsilon_1^2}{8Z^2} \kappa \xi^3 E_g [Z\tilde{r}^2 - (3Z-4)\tilde{z}^2], \quad (49)$$

$$\delta V_{\theta 1} = \frac{Z}{4} g e \xi^2 E_g L_z, \quad (50)$$

$$\delta W_{\theta 1} = \frac{1-Z}{2} g e \xi^2 E_g S_z, \quad (51)$$

where we have defined the rescaled coordinates  $\tilde{x}_i \equiv (Z/\varepsilon_1)(x_i/a_0)$ .

According to the statement of the problem, we are considering a hydrogenlike ion embedded in a medium with optical properties  $(\varepsilon_1, \mu_1)$  at a distance  $b$  from a planar topological insulator characterized by its optical properties  $(\varepsilon_2, \mu_2)$  and the TMEP  $\theta$ , as shown in Fig. 1. Without loss of generality, we can restrict our analysis to the case  $\mu_1 = \mu_2 = 1$ , which is suitable for both conventional and topological insulators. Furthermore, we observe that the potentials  $\delta V_{\theta 1}$  and  $\delta W_{\theta 1}$  are exclusively of topological origin in the sense that they vanish for  $\theta = 0$ . On the contrary, the optical and topological properties coexist for the potentials  $\delta U_1$  and  $\delta U_2$  provided  $\varepsilon_1 \neq \varepsilon_2$  since they depend on  $\kappa$ , defined in Eq. (11). Therefore, one can consider the following two interesting cases: (a)  $\varepsilon_1 = \varepsilon_2$  and (b)  $\varepsilon_1 \neq \varepsilon_2$ . In the former case, we consider the ion to be embedded in a dielectric medium with the same optical properties that those of the TI, such that the electrostatic effects are suppressed and only the topological ones become important. The second case is perhaps the most realistic situation from the experimental point of view since spectroscopy experiments consider the atoms in vacuum. On the other hand, from the potentials (48)–(51) we can also distinguish two situations of interest, i.e., (i)  $Z \neq 1$  (hydrogenlike ions) and (ii)  $Z = 1$  (hydrogen atom). The fundamental difference arises from the fact that potentials  $\delta U_1$  and  $\delta W_{\theta 1}$  vanish for the hydrogen atom case. In the next sections, we discuss the lowest lying energy levels, in each case, where the TME effects become manifest.

#### IV. ENERGY SHIFTS OF THE SPECTRUM OF HYDROGENLIKE IONS

##### A. General considerations

In this section, we work out the energy shifts on the hyperfine structure states of hydrogenlike ions due to the Casimir-Polder interaction  $\delta U_1 + \delta U_2 + \delta V_{\theta 1} + \delta W_{\theta 1}$ . We study the cases described in the end of the previous section but we left the case of the hydrogen atom in vacuum for a detailed analysis in the next section.

In our notation, the electron variables are labeled by the quantum numbers  $n, \ell, s, j$ , and  $m_j$ , where the total electron angular momentum  $\mathbf{J} = \mathbf{L} + \mathbf{S}$  is labeled by  $j = \ell \pm s$ , with  $\ell$  being the orbital angular momentum quantum number and

$s = 1/2$  its spin. Explicit forms for the fine structure states, abbreviated as  $|j, m_j\rangle_{\text{fs}} \equiv |n, \ell, s, j, m_j\rangle$ , are

$$|j, m_j\rangle_{\text{fs}} = \sum_{m_s=-s}^{+s} \langle \ell, s, m_j - m_s, m_s | j, m_j \rangle \times |n, \ell, m_j - m_s\rangle \otimes |s, m_s\rangle_e, \quad (52)$$

where the  $|n, \ell, m\rangle$  are the spinless Coulomb bound states with  $\langle \mathbf{r} | n, \ell, m \rangle = R_{n\ell}(r) Y_\ell^m(\vartheta, \varphi)$ , and the  $|s, m_s\rangle_e$  are the electron spin states. The required Clebsch-Gordan (CG) coefficients are given by

$$\langle \ell, s, m_j \mp s, \pm s | j = \ell + s, m_j \rangle = \sqrt{\frac{1}{2} \pm \frac{m_j}{2\ell + 1}},$$

$$\langle \ell, s, m_j \mp s, \pm s | j = \ell - s, m_j \rangle = \mp \sqrt{\frac{1}{2} \mp \frac{m_j}{2\ell + 1}}. \quad (53)$$

The states  $|n, \ell, s, j, m_j\rangle$  are, by construction, simultaneous eigenfunctions of  $\mathbf{L}^2, \mathbf{S}^2, \mathbf{J}^2$ , and  $J_z$ .

At the hyperfine level, we must include the nuclear spin  $i$ . The total atomic angular momentum  $\mathbf{F} = \mathbf{J} + \mathbf{I}$  has quantum number  $f$  satisfying  $|j - i| \leq f \leq |j + i|$ . It is conserved due to rotational symmetry, so the states having different eigenvalues  $m_f$  of  $F_z$  would be degenerate in the absence of an external magnetic field, but all other degeneracies are broken. The hyperfine structure states, abbreviated as  $|j, f, m_f\rangle_{\text{hfs}} \equiv |n, \ell, s, j, f, m_f\rangle$ , have the form

$$|j, f, m_f\rangle_{\text{hfs}} = \sum_{m_i=-i}^{+i} \langle j, i, m_f - m_i, m_i | f, m_f \rangle \times |j, m_f - m_s\rangle_{\text{fs}} \otimes |i, m_i\rangle_N, \quad (54)$$

where  $|i, m_i\rangle_N$  are the nuclear spin states. The CG coefficients in Eq. (54) depend on the value of the nuclear spin. For hydrogenlike ions with  $i = 1/2$  we have  $f = j \pm 1/2$ , and the CG coefficients are given by (53) with the replacement  $\{s, j, \ell, m_j\} \rightarrow \{i, f, j, m_f\}$ . For spin  $i > 1/2$  the expressions for the CG coefficients are simple but more cumbersome than those appearing in (53). The radial contribution of the hyperfine states, which we take as the radial functions  $R_{n\ell}$  of the Coulomb potential  $-Ze^2/\varepsilon_1 r$ , are the zeroth-order approximation of the full eigenfunctions in the Hamiltonian including the fine and hyperfine structure contributions, with their first-order correction being of the order  $\alpha^2$ . Since all terms in the potentials (48)–(51) are already of higher order, this approximation is enough to compute the lowest order additional energy shifts.

We are start by perturbing the hyperfine atomic spectrum, which is nondegenerate except for the quantum number  $m_f$ , so that the potential  $\delta U_1$  does not contribute to the first-order energy shifts since it is a first-rank spherical tensor. Nevertheless, it contributes to second-order shifts, but its order of magnitude will be suppressed by a factor of  $\alpha^2 \sim 10^{-5}$  with respect to the other potentials (49)–(51) for  $b \sim \mu\text{m}$ . Thus, in the following we do not consider such terms. In a similar fashion, although the potential  $\delta U_2$  contributes both to first- and second-order energy shifts, it is sufficient to consider only the former contribution. The perturbation  $\delta U_2$  does not depend on the nuclear spin and its expectation value can be directly

computed in the hyperfine structure basis. The result is

$$\frac{\langle \delta U_2 \rangle}{E_g} = -\frac{\kappa \xi^3}{8} \left( \frac{\varepsilon_1}{Z} \right)^2 \langle \tilde{r}^2 \rangle_{n\ell} \Sigma_Z^{ijf m_f}, \quad (55)$$

where

$$\langle \tilde{r}^2 \rangle_{n\ell} = \frac{1}{2} n^2 [5n^2 - 3\ell(\ell + 1) + 1], \quad (56)$$

$$\Sigma_Z^{ijf m_f} = Z - (3Z - 4) \langle \cos^2 \vartheta \rangle_{\text{hfs}}^{ijf m_f}. \quad (57)$$

The expectation value in the hyperfine structure basis can be computed in terms of those in the fine structure basis as

$$\begin{aligned} \langle \cos^2 \vartheta \rangle_{\text{hfs}}^{ijf m_f} &= \sum_{m_i=-i}^{+i} \langle j, i, m_f - m_i | f, m_f \rangle^2 \\ &\times \langle \cos^2 \vartheta \rangle_{\text{fs}}^{j, m_f - m_i}, \end{aligned} \quad (58)$$

where

$$\langle \cos^2 \vartheta \rangle_{\text{fs}}^{j, m_j} = \frac{j(j+1) - m_j^2}{2j(j+1)}. \quad (59)$$

The final form of Eq. (58) strongly depends on the value of the nuclear spin. For example, for  $i = 1/2$  we have  $f = j \pm i$ , and a simple calculation yields

$$\langle \cos^2 \vartheta \rangle_{\text{hfs}}^{ijf m_f} = \frac{1}{2} - \frac{1 + 4m_f^2}{8j(j+1)} \pm' \frac{m_f^2}{j(j+1)(2j+1)}. \quad (60)$$

Analogous expressions for nuclear spin  $i > 1/2$  can be obtained in a similar manner.

The energy shifts arising from the Zeeman-like potentials (50) and (51) can be computed in a simple fashion. We consider the potential

$$\delta V_\theta \equiv \delta V_{\theta 1} + \delta W_{\theta 1} = \frac{Z}{4} g e \xi^2 E_g V_z, \quad (61)$$

where we have defined the operator

$$\mathbf{V} = \mathbf{L} - 2 \frac{Z-1}{Z} \mathbf{S}. \quad (62)$$

We observe that the perturbation potential  $\delta V_\theta$  is of topological origin, since it vanishes for  $\theta = 0$ , and therefore it is a signature of the topological nontriviality of the TIs and particularly of the image magnetic monopole effect. We are in a subspace of fixed  $n$ ,  $\ell$ ,  $j$ , and  $s$ , so we can use the Wigner-Eckart theorem to make the replacement  $V_z = g_{\text{fs}}^{(Z)} J_z$ , provided we never compute matrix elements between states with different  $j$ . Here  $g_{\text{fs}}^{(Z)} = \langle \mathbf{J} \cdot \mathbf{V} \rangle / j(j+1)$  is a fine-structure type  $g$  factor. Since we are also in a subspace with fixed  $f$ , we can use Wigner-Eckart theorem again to take  $J_z = g_{\text{hfs}} F_z$ , where  $g_{\text{hfs}} = \langle \mathbf{J} \cdot \mathbf{F} \rangle / f(f+1)$  is the usual hyperfine-structure  $g$  factor. Therefore, the perturbation  $\delta V_\theta$  lifts the degeneracy between hyperfine levels with equal  $f$  and unequal  $m_f$  in a linear fashion, giving energy shifts

$$\langle \delta V_\theta \rangle = \frac{Z}{4} g e \xi^2 E_g g_{\text{fs}}^{(Z)} g_{\text{hfs}} m_f, \quad (63)$$

where the  $g$  factors are given by

$$\begin{aligned} g_{\text{fs}}^{(Z)} &= \frac{1}{2Z} \left[ (2-Z) + (3Z-2) \frac{\ell(\ell+1) - s(s+1)}{j(j+1)} \right], \\ g_{\text{hfs}} &= \frac{1}{2} \left[ 1 + \frac{j(j+1) - i(i+1)}{f(f+1)} \right]. \end{aligned} \quad (64)$$

Now let us discuss the conditions under which the energy shifts (63) induced by the TME are comparable with the nonperturbed hyperfine spectrum for different cases. To this end, we consider the expression for the hyperfine splitting of a one-electron ion [43]

$$E_{\text{hfs}} = \frac{\alpha(\alpha Z)^3}{\varepsilon^3 n^3} g_\mu \frac{m_e^2}{m_p} \frac{f(f+1) - i(i+1) - j(j+1)}{2j(j+1)(2\ell+1)}, \quad (65)$$

where  $m_p$  is the proton mass,  $g_\mu = \mu / (\mu_N i)$ ,  $\mu$  is the nuclear magnetic moment, and  $\mu_N$  is the nuclear magneton. In the above, we have neglected the relativistic corrections together with the nuclear charge distribution correction, the Bohr-Weisskopf correction, and the radiative corrections. Also, we have incorporated the effect of the dielectric medium with permittivity  $\varepsilon$ .

From Eqs. (55) and (63), we find two different regimes to be analyzed separately. On the one hand, we observe that for nucleus-surface distances of the order of micrometers ( $b \sim \mu\text{m}$ ), the topological contributions are suppressed with respect to the standard electromagnetic ones ( $\theta = 0$ ) provided  $\varepsilon_1 \neq \varepsilon_2$ . On the other hand, we can see that the case  $\varepsilon_1 = \varepsilon_2$  enhance the topological contribution (63), and thus it deserves a separate analysis. Next, we analyze the cases mentioned above. Let us consider both (a) the lowest and (b) the highest lines where the TME becomes manifest, that is, the ground state  $1S_{1/2}$  and the circular Rydberg states, respectively. For definiteness, in the sequel we restrict our analysis to the recently discovered topological insulator TlBiSe<sub>2</sub> for which  $\varepsilon_2 = 4$  and  $\mu_2 = 1$ , and we left  $\theta$  as a free parameter.

## B. Case $\varepsilon_1 = \varepsilon_2$

When the hydrogenlike ion is embedded in a medium with the same optical properties of the TI, i.e.,  $\varepsilon_1 = \varepsilon_2 \equiv \varepsilon$ , the energy shifts are given by Eqs. (55) and (63) together with

$$\kappa = -\frac{\tilde{\theta}^2}{4\varepsilon^2}, \quad eg = \frac{\alpha\tilde{\theta}}{2\varepsilon}, \quad (66)$$

where we have considered that  $\varepsilon \gg \alpha^2$ .

### 1. The ground state $1S_{1/2}$

The hyperfine spectrum for the ground state  $1S_{1/2}$  is

$$E_{\text{hfs}}^{1S_{1/2}} = \frac{Z^3}{\varepsilon^3} \Lambda g_\mu [f(f+1) - i(i+1) - 3/4], \quad (67)$$

where  $\Lambda \equiv (4/3) |E_g| \alpha^2 (m_e/m_p) = 5.25 \times 10^{-7} \text{ eV} = 1.27 \times 10^8 \text{ Hz}$ . One can further check that Eq. (67) correctly yields the 21-cm line arising from the transition between the states with  $f = 1$  and  $f = 0$  in hydrogen, for which  $i = 1/2$ ,  $g_\mu = 5.56$ , and  $Z = 1$ . On the other hand, from Eq. (63) together



with Eq. (66) the topological contribution gives

$$\langle \delta V_\theta \rangle_{1S_{1/2}} = \Gamma \frac{Z-1}{\varepsilon} (\theta/\pi) m_f \left[ \frac{f(f+1) - i(i+1) + 3/4}{f(f+1)} \right], \quad (68)$$

where  $\Gamma \equiv |E_g| \alpha^2 \xi^2 / 8 = 2.57 \times 10^{-13} \text{ eV} = 62.2 \text{ Hz}$  for  $b \sim \mu\text{m}$ . The ratio between the hyperfine spectrum and the topological contribution for an hydrogenlike ion for which  $i = 1/2$ ,  $f = 1$ , and  $m_f = \pm 1$  is

$$r_{\theta\text{-hfs}}^{1S_{1/2}} = \frac{|\langle \delta V_\theta \rangle_{1S_{1/2}}|}{|E_{\text{hfs}}^{1S_{1/2}}|} = \frac{|\theta/\pi| Z-1}{g_\mu Z^3} (1.5 \times 10^{-5}). \quad (69)$$

One can further check that  $r_{\theta\text{-hfs}}^{1S_{1/2}}$  has a maximum at  $Z = 3/2$  and decreases as increasing  $Z$ , thus implying that hydrogenlike ions with small values  $Z$  are the best probes to test the TME in its ground state. Consider, for example, the  ${}^3\text{He}^+$  ion, for which  $Z = 2$ ,  $i = 1/2$ , and  $\mu/\mu_N = 1.15$ . In this case, the ratio (69) becomes  $r_{\theta\text{-hfs}}^{1S_{1/2}} = |\theta/\pi| (3.4 \times 10^{-6})$ , which is small enough to be measured for appropriate values of the TMEP. For heavy ions, such as  ${}^{207}\text{Pb}^{81+}$ , for which  $Z = 82$ ,  $i = 1/2$ , and  $\mu/\mu_N = 0.587$ , we find  $r_{\theta\text{-hfs}}^{1S_{1/2}} = |\theta/\pi| (7.5 \times 10^{-9})$ , which is even smaller than those for the  ${}^3\text{He}^+$  ion.

## 2. Circular Rydberg states

Now let us consider the case of circular Rydberg hydrogenlike ions, i.e., highly excited states with its quantum numbers maximally projected. We define the circular states as  $|n\rangle_{\text{circ}} = |n, \ell_{\text{max}} = n-1, j_{\text{max}} = \ell_{\text{max}} + 1/2, f_{\text{max}} = j_{\text{max}} + i, m_{f_{\text{max}}} = f_{\text{max}}\rangle$ . Adapting the approach of Ref. [44] for Rydberg hydrogen to our case, we obtain a retardation line given by

$$|\delta E_r| = \frac{Z^2}{\varepsilon^2 n^3} (6.58 \times 10^{15} \text{ Hz}) \quad (70)$$

$$L_r = \frac{\varepsilon^2 n^3}{Z^2} (4.56 \times 10^{-2} \mu\text{m}). \quad (71)$$

According to Eq. (65) the energy difference  $\Delta E_{\text{hfs}}^{\text{circ}}$  between neighboring hyperfine circular Rydberg states  $|n\rangle_{\text{circ}}$  and  $|n-1\rangle_{\text{circ}}$  is

$$\Delta E_{\text{hfs}}^{\text{circ}} = \frac{5i g_\mu Z^3}{n^6 \varepsilon^3} (4.76 \times 10^8 \text{ Hz}). \quad (72)$$

Our main concern is with the energy shifts  $\delta U_2$  and  $\delta V_\theta$  given by Eqs. (55) and (63), respectively. In our approximation, which is that of circular Rydberg states embedded in a medium with the same optical properties to that of the TI, we find that  $g_{\text{hfs}} = g_{\text{fs}}^{(Z)} = 1$ , from which we establish the following ratio:

$$r_{\theta\text{-hfs}}^{\text{circ}} \equiv \frac{|\langle \delta V_\theta \rangle|}{\Delta E_{\text{hfs}}^{\text{circ}}} = \frac{(\theta/\pi) \varepsilon^2 \xi^2 n^7 m_p}{40 Z^2 i g_\mu m_e}. \quad (73)$$

In a similar fashion, we can also establish an expression for the ratio between the maximum energy shift  $|\langle \delta U_2 \rangle_{\text{max}}|$ , which is obtained from Eq. (55) together with  $\langle \cos^2 \vartheta \rangle = 1$  and  $\langle \vec{r}^2 \rangle = n^4$ , and the hyperfine energy  $\Delta E_{\text{hfs}}^{\text{circ}}$ . We obtain

$$r_{U\text{-hfs}}^{\text{circ}} \equiv \frac{|\langle \delta U_2 \rangle_{\text{max}}|}{\Delta E_{\text{hfs}}^{\text{circ}}} = \frac{(\theta/\pi)^2 \varepsilon^3 \xi^3 n^{10} m_p}{80 Z^4 i g_\mu m_e}. \quad (74)$$

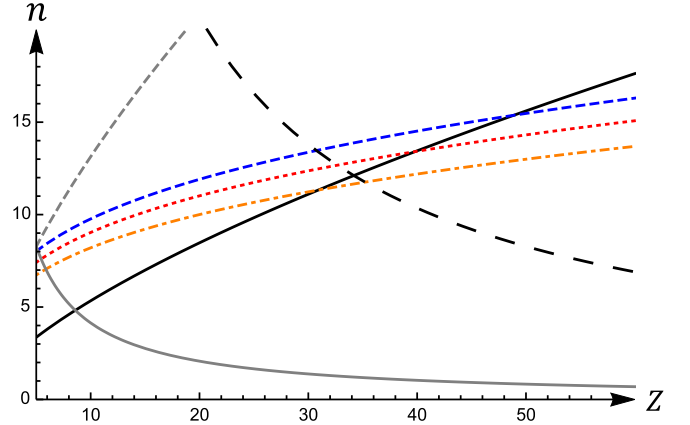


FIG. 2. Parameter region  $n(Z)$ , for  $b = B_{\text{min}}$ , for detecting the TME in circular Rydberg hydrogenlike ions for  $\varepsilon_1 = \varepsilon_2$ . The meaning of each line is given in the text.

We observe that high values of the TMEP  $\theta$  favor the ratios (73) and (74); therefore we take  $\theta = 11\pi$  hereafter. Using the numerical values  $\varepsilon = 4$  and  $m_p/m_e = 1840$ , we find that the ratios become

$$r_{\theta\text{-hfs}}^{\text{circ}} = \frac{\xi^2 n^7}{i g_\mu Z^2} (8 \times 10^3), \quad r_{U\text{-hfs}}^{\text{circ}} = \frac{\xi^3 n^{10}}{i g_\mu Z^4} (3.6 \times 10^5). \quad (75)$$

We now come to the problem of choosing an adequate value for  $b$ . The lowest value of  $b$  which will make the ratios (75) as high as possible is limited by the thickness  $w \approx 6 \times 10^{-3} \mu\text{m}$  ( $\xi \approx 10^{-2}$ ) of the magnetic coating, but more importantly by the experimental possibilities. Motivated by the works in Refs. [32] we take  $b \leq \mu\text{m}$  and explore the range  $B_{\text{min}} < b < B_{\text{max}}$ , where  $B_{\text{min}} = 0.265 \mu\text{m}$  and  $B_{\text{max}} = 1.1 \mu\text{m}$ . Notice that for  $b = B_{\text{min}}$ , we have  $b = 44.2 w$ , which is still larger than the width of the magnetic coating. Now let us discuss the allowed parameter region for  $b = B_{\text{min}}$ .

By imposing the nonretarded constraint  $B_{\text{max}} \leq L_r$ , we obtain the condition  $n \geq 1.15 Z^{2/3}$ , which corresponds to the continuous black line in Fig. 2. Since the energy shifts must be smaller than the unperturbed energy spectrum, we must consider that  $r_{\theta\text{-hfs}}^{\text{circ}} < 1$ , thus providing the condition  $n \leq 3.97 (i g_\mu Z^2)^{1/7}$  for  $b = B_{\text{min}}$ . In Fig. 2, we show the latter condition for  $i g_\mu = 5.53$  (blue dashed line),  $i g_\mu = 3.18$  (red dotted line), and  $i g_\mu = 1.62$  (orange dot-dashed line), which fall within the nonretarded region for  $Z \leq 49, 39, 30$ , respectively. We have chosen the values for  $i g_\mu$  from Ref. [43]. In Fig. 2, we also show the curves  $n(Z)$  corresponding to the lower limits of the regions satisfying  $|\langle \delta V_\theta \rangle| > 10^6 \text{ Hz}$  (black large dashed line) and  $|\langle \delta V_\theta \rangle| > 10^5 \text{ Hz}$  (continuous gray line) for  $b = B_{\text{min}}$ . One can further verify that the condition  $|\langle \delta V_\theta \rangle| > 10^6 \text{ Hz}$  for  $b = B_{\text{max}}$  selects values of  $n$  larger than 100 for the whole interval  $1 < Z < 100$ , and this is why we have restricted ourselves to  $b = B_{\text{min}}$  as a reasonable lower limit for  $b$ . The region below the gray dashed line corresponds to the condition  $r_{\theta\text{-hfs}}^{\text{circ}} > 10 r_{U\text{-hfs}}^{\text{circ}}$  for  $b = B_{\text{min}}$ , while the case  $r_{\theta\text{-hfs}}^{\text{circ}} > r_{U\text{-hfs}}^{\text{circ}}$  is not shown in the figure since it lies higher than the gray dashed line. For the ions listed in Table 3 of Ref. [43],

TABLE I. The quantum number for different heavy hydrogenlike ions satisfying  $r_{\theta\text{-hfs}}^{\text{circ}} = 1$ .

Ion	$Z$	$\mu/\mu_N$	$i$	$n$
$^{133}\text{Cs}^{54+}$	55	2.5825	7/2	20
$^{159}\text{Tb}^{64+}$	65	2.014	3/2	20
$^{207}\text{Pb}^{81+}$	82	0.587	1/2	18
$^{235}\text{U}^{91+}$	92	0.39	7/2	18

we find that the maximum value for the TME correction is  $|\langle\delta V_\theta\rangle| = 1.83 \times 10^6$  Hz for  $^{113}\text{In}^{48+}$ .

To close this section, we remark that the topological Zeeman-type energy shifts can be of the same order of magnitude as that of the hyperfine energy levels of a hydrogenlike atom embedded in a medium with the same dielectric constant as that of the TI. From Eq. (73), we have

$$n = 5.59 \times \sqrt[7]{\left(\frac{\mu}{\mu_N}\right) Z^2} \quad (76)$$

for  $r_{\theta\text{-hfs}}^{\text{circ}} = 1$ . In Table I, we present the values of the principal quantum number which solve Eq. (76) for different circular states of hydrogenlike heavy ions.

### C. Case $\varepsilon_1 \neq \varepsilon_2$

Now let us consider the atom to be embedded in a medium with different optical properties to that of the TI, i.e.,  $\varepsilon_1 \neq \varepsilon_2$ . For definiteness, here we consider the atom in a vacuum, such that the basic parameters now become

$$\kappa = \frac{1 - \varepsilon_2}{1 + \varepsilon_2}, \quad eg = \frac{\alpha^2(\theta/\pi)}{1 + \varepsilon_2}, \quad (77)$$

where we used that  $\tilde{\theta}^2 \ll 1$ . We observe that  $|eg/\kappa| \sim 2 \times 10^{-4}$  for the TI TlBiSe<sub>2</sub>; therefore, contrary to the previous situation in Sec. IV B, the topological correction  $\langle\delta V_\theta\rangle$  will be much suppressed with respect to the optical correction  $\langle\delta U_2\rangle$ .

#### 1. The ground state $1S_{1/2}$

Using the hyperfine structure energy levels together with the Zeeman-type energy shifts for the ground state  $1S_{1/2}$ , we find the ratio

$$t_{\theta\text{-hfs}}^{1S_{1/2}} = \frac{|\langle\delta V_\theta\rangle_{1S_{1/2}}|}{|E_{\text{hfs}}^{1S_{1/2}}|} = \frac{|\theta/\pi| Z - 1}{g_\mu Z^3} (8 \times 10^{-8}), \quad (78)$$

which is three orders of magnitude smaller than those of Eq. (69). Therefore, the ground state of a hydrogenlike ion in the vacuum is not a good probe to test the TME.

#### 2. Circular Rydberg states

The energy difference  $\Delta E_{\text{hfs}}^{\text{circ}}$  between neighboring hyperfine circular Rydberg states  $|n\rangle_{\text{circ}}$  and  $|n-1\rangle_{\text{circ}}$  is given by Eq. (72) with  $\varepsilon = 1$ . On the other hand, in the approximation we are working with, together with the choice of the parameters (77) of this case, we find the energy shifts  $\langle\delta U_2\rangle$  and  $\langle\delta V_\theta\rangle$  to be

$$|\langle\delta U_2\rangle| = 1974 \frac{n^4}{Z} \text{ Hz}, \quad |\langle\delta V_\theta\rangle| = 2408 n Z \text{ Hz}, \quad (79)$$

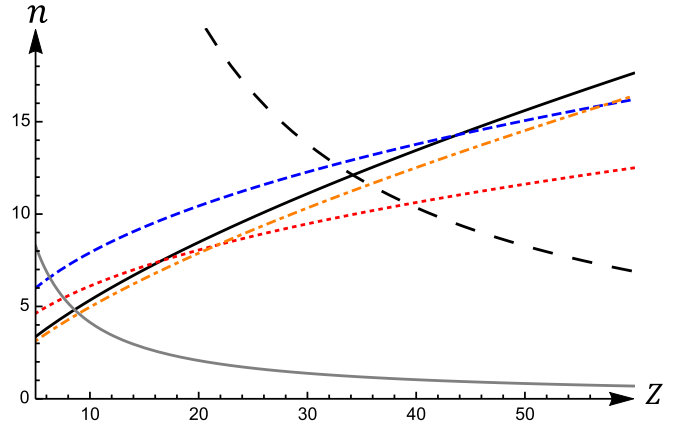


FIG. 3. Parameter region  $n(Z)$ , for  $b = B_{\text{min}}$ , for detecting the TME in circular Rydberg hydrogenlike ions for  $\varepsilon_1 \neq \varepsilon_2$ . The meaning of each line is given in the text.

where we have used that  $g_{\text{hfs}} = g_{\text{fs}}^{(Z)} = 1$ ,  $\langle\tilde{r}^2\rangle = n^4$ , and  $\theta = 11\pi$ . The ratios between the energy shifts (79) and the hyperfine energy difference  $\Delta E_{\text{hfs}}^{\text{circ}}$  read

$$t_{\theta\text{-hfs}}^{\text{circ}} = \frac{n^7}{i g_\mu Z^2} (1 \times 10^{-6}), \quad t_{U\text{-hfs}}^{\text{circ}} = \frac{n^{10}}{i g_\mu Z^4} (8.3 \times 10^{-7}), \quad (80)$$

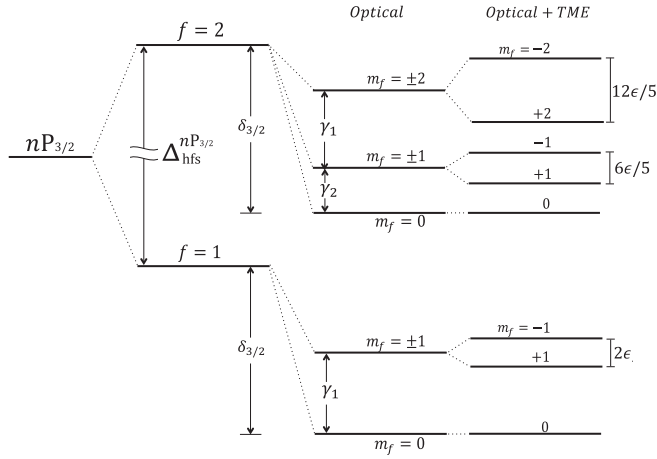
for  $b = B_{\text{min}} = 0.265 \mu\text{m}$ . Now let us analyze the parameter region  $n-Z$ . We first recall that the nonretarded constraint  $B_{\text{min}} < L_r$  provides the condition  $n > 1.15 Z^{2/3}$ , which corresponds to the continuous black line in Fig. 3.

By imposing the energy shifts to be smaller than the unperturbed energy spectrum, i.e.,  $t_{\theta\text{-hfs}}^{\text{circ}} < 1$ , we find the condition  $n \leq 2.67 (i g_\mu Z^4)^{1/10}$  for  $b = B_{\text{min}}$ . Using Table 3 in Ref. [43] for the properties of different hydrogenic ions, in Fig. 3 we show the latter condition for the largest (blue dashed line) and the lowest (red dotted line) values of  $i g_\mu$ , respectively. On the other hand, the condition  $t_{\theta\text{-hfs}}^{\text{circ}} \leq t_{U\text{-hfs}}^{\text{circ}}$  produces the region  $n \geq 1.07 Z^{2/3}$ , which corresponds to the orange dot-dashed line in Fig. 3.

Figure 3 shows that the condition  $t_{\theta\text{-hfs}}^{\text{circ}} = t_{U\text{-hfs}}^{\text{circ}}$  is below to the retardation line (continuous black line), in such a way that here we always have  $t_{\theta\text{-hfs}}^{\text{circ}} < t_{U\text{-hfs}}^{\text{circ}}$ . The region between the large black dashed and the continuous gray lines corresponds to  $10^6 \text{ Hz} < |\langle\delta V_\theta\rangle| < 10^7 \text{ Hz}$ . Therefore, we observe that the condition  $\varepsilon_1 \neq \varepsilon_2$  places a strong restriction upon the allowed parameter region, when compared with the similar situation in the case  $\varepsilon_1 = \varepsilon_2$ .

## V. ENERGY SHIFTS IN THE HYDROGEN SPECTRUM

The optical and Zeeman-type energy shifts for hydrogen can be directly obtained from Eqs. (55) and (63), respectively, by taking  $i = s = 1/2$  and  $Z = 1$ . We observe that the Zeeman splitting  $E_\theta$  vanishes for  $S$  states since  $g_{\text{fs}}^{(1)} = 0$ . Therefore, the lowest lying lines for which the TME becomes manifest are the  $P$  states. In the following, we discuss the spectroscopic transitions for the  $nP_{3/2}$  and  $nP_{1/2}$  lines.


 FIG. 4. Splitting of the  $nP_{3/2}$  line.

### A. Spectroscopy of the $nP_{3/2}$ states

In this particular case, we take the set of quantum numbers  $\{s, \ell, j, i\} = \{1/2, 1, 3/2, 1/2\}$ , such that the atomic angular momentum can take the values  $f = 3/2 \pm 1/2$ . The optical energy shifts then become

$$\langle \delta U_{2\pm'} \rangle^{nP_{3/2}} = \frac{\kappa \epsilon_1^2 \xi^3}{48} |E_g| n^2 (n^2 - 1) (22 - 2m_f^2 \pm' m_f^2), \quad (81)$$

where the values of  $m_f$  are restricted by  $-f \leq m_f \leq f$ . The Zeeman-like energy shifts take the form

$$\langle \delta V_{\theta\pm'} \rangle^{nP_{3/2}} = \frac{g e \xi^2}{24} E_g (4 \mp' 1) m_f. \quad (82)$$

Also, from Eq. (65) one can further obtain that the unperturbed hyperfine energy levels are

$$E_{\text{hfs}}^{nP_{3/2}} = \frac{\Gamma_{3/2}}{n^3} [f(f+1) - 9/2], \quad (83)$$

where  $\Gamma_{3/2} = 1.95 \times 10^{-7}$  eV. In Fig. 4, we present the general energy shifts of the  $nP_{3/2}$  line in two steps. We first observe that the optical contribution (81) partially breaks the degeneracies of the hyperfine levels, but the degeneracy of the levels with  $m_f \neq 0$  is still present. Finally we add the contributions from  $\langle \delta V_{\theta\pm'} \rangle^{nP_{3/2}}$  arising from the TME and observe that this effect completely breaks the degeneracy of the hyperfine states  $|j, f, m_f\rangle_{\text{hfs}}$ . The values of the parameters appearing in Fig. 4 are

$$\begin{aligned} \delta_{3/2} &= 22(\gamma_1/3) = 22\gamma_2 = \frac{11}{24} \epsilon_1^2 \xi^3 |\kappa E_g| n^2 (n^2 - 1), \\ \epsilon &= \frac{5}{24} |g e E_g| \xi^2, \quad \Delta_{\text{hfs}}^{nP_{3/2}} = \frac{4}{n^3} \Gamma_{3/2}. \end{aligned} \quad (84)$$

In the following, we determine the parameter region where our results are included. To the best of our knowledge, the hyperfine splitting of the lines  $nP_{3/2}$  has not yet been measured and the existing data correspond to theoretical calculations, which produce the value  $\Delta_{\text{hfs}}^{nP_{3/2}}$  together with a theoretical uncertainty  $\Delta_{\text{tu}}^{nP_{3/2}}$  [45,46]. In order for our results to be

accessible from a theoretical perspective, we have to identify a range of distances for  $b$  satisfying the following conditions: (i) On one hand,  $b$  should be such that the additional distance-dependent energy shifts (81) and (82) are larger than the theoretical uncertainty  $\Delta_{\text{tu}}^{nP_{3/2}}$ , but smaller than the corresponding hyperfine splitting  $\Delta_{\text{hfs}}^{nP_{3/2}}$ , and (ii) on the other hand,  $b$  should be larger than the thickness of the magnetic coating covering the TI surface (to ensure a negligible wave-function overlap) and smaller than the wavelength  $\lambda_C$  of a typical hyperfine transition (to ensure the validity of the nonretarded regime). Typically  $\lambda_C \sim \text{m}$ , while a ferromagnetic covering for the TI (such as GdN) can be grown as a thin film of thickness  $\sim 6 \text{ nm}$  [23]. Thus,  $b \sim \mu\text{m}$  satisfies the required conditions in practical terms. This choice will restrict the possible values for the remaining parameters in the energy shifts, namely the principal quantum number  $n$  and the permittivities  $\epsilon_1$  and  $\epsilon_2$ . Our primary interest here is to accommodate the Zeeman-type splitting  $\langle \delta V_{\theta\pm'} \rangle^{nP_{3/2}}$ , which does not depend on  $n$  but depends inversely on the permittivities. Thus low values of  $\epsilon_1$  and  $\epsilon_2$  favor this contribution. Taking into account the above considerations, we find that the recently discovered topological insulator TlBiSe<sub>2</sub>, for which  $\theta = \pi$ ,  $\mu = 1$ , and  $\epsilon \approx 4$  [47–49], is a good candidate to illustrate our procedure. Assuming that the dielectric medium has also a low permittivity, we find that the Zeeman-type energy splitting  $2\epsilon$  is of the order of  $10^{-12}$  eV, while the maximum optical splitting  $\gamma_1 + \gamma_2$  becomes of the order of  $n^2(n^2 - 1) \times 10^{-12}$  eV for  $\epsilon_1 \neq \epsilon_2$  and  $n^2(n^2 - 1) \times 10^{-16}$  eV for  $\epsilon_1 = \epsilon_2$ . Now, since we have computed the energy shifts from a perturbative perspective, we must guarantee the validity of perturbation theory by imposing the energy splitting  $2\epsilon$  and  $\gamma_1 + \gamma_2$  to be at least three orders of magnitude smaller than  $\Delta_{\text{hfs}}^{nP_{3/2}}$ , thus restricting the possible values for the principal quantum number  $n$ . Therefore, from (84) we can see that  $n = 2$  is the best option for the  $\epsilon_1 \neq \epsilon_2$  case, since  $\Delta_{\text{hfs}}^{2P_{3/2}} = 9.75 \times 10^{-8}$  eV and  $\Delta_{\text{tu}}^{2P_{3/2}} = 2.47 \times 10^{-12}$  eV, thus having a range of four orders of magnitude to accommodate the energy shifts. For the case  $\epsilon_1 = \epsilon_2$ , one can choose  $n = 10$  such that  $\gamma_1 + \gamma_2 \approx \Delta_{\text{hfs}}^{10P_{3/2}} \times 10^{-3}$ ; however, in this case the energy shifts become smaller than the theoretical uncertainty. Therefore, based on the previous analysis, for definiteness let us consider the atom to be in vacuum in front of the TI TlBiSe<sub>2</sub> and consider the energy shifts on the  $2P_{3/2}$  line.

Using the previously chosen set of parameters, we establish the functions  $\Delta U \equiv \gamma_1 + \gamma_2 = (3/5)|E_g|\xi^3$  and  $\Delta V_{\theta} \equiv 2\epsilon = (1/12)|(\theta/\pi)E_g|\alpha^2\xi^2$  for the maximum optical and Zeeman-type splitting, respectively. By imposing  $\Delta U = \Delta_{\text{hfs}}^{2P_{3/2}} \times 10^{-3}$  we determine  $b \sim 4337a_0 = 0.23 \mu\text{m}$ , which is a distance perfectly achievable with current experimental techniques. In Fig. 5, we present a log-log plot of  $\Delta U$  (black line) and  $\Delta V_{\theta}$ , for two cases:  $\theta = \pi$  (dashed red line) and  $\theta = 11\pi$  (dotted blue line). The green (upper) and orange (lower) shaded regions are forbidden by the upper bound  $\Delta_{\text{hfs}}^{2P_{3/2}}$  of the hyperfine structure and by the lower bound arising from the theoretical uncertainty  $\Delta_{\text{tu}}^{2P_{3/2}}$ , respectively. We observe that the Zeeman-type contributions, although smaller than the optical one, are bigger than the theoretical uncertainty associated with the determination of the hyperfine splitting of the  $2P_{3/2}$  state. For  $\theta = \pi$ , we find  $\Delta V_{\pi} = 3.15 \times 10^{-12}$  eV,

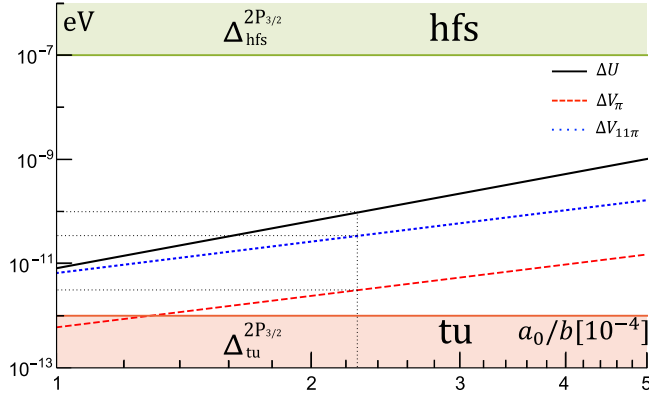


FIG. 5. Region of accessibility for detecting the TME in hydrogen. The green (upper) and orange (lower) shaded regions are forbidden by the hyperfine splitting and the theoretical uncertainty of the  $2P_{3/2}$  line, respectively. The selected value of  $b$  is  $0.23 \mu\text{m}$ .

while for  $\theta = 11\pi$  we have  $\Delta V_{11\pi} = 3.47 \times 10^{-11}$  eV. The resulting values of the parameters (84) are  $\delta_{3/2} = 133$  kHz,  $\gamma_1 = 18$  kHz,  $\gamma_2 = 3$  kHz, and  $\epsilon = 388$  Hz for  $\theta = \pi$  and  $\epsilon = 4.2$  kHz for  $\theta = 11\pi$ .

### B. Spectroscopy of the $nP_{1/2}$ states

Now we consider the set of quantum numbers  $\{s, \ell, j, i\} = \{1/2, 1, 1/2, 1/2\}$ , such that the atomic angular momentum can take the values  $f = 1/2 \pm 1/2$ . The energy shifts can be obtained directly from Eqs. (55) and (63) in a simple fashion. For the optical energy shifts, one finds

$$\langle \delta U_2 \rangle^{nP_{1/2}} = \frac{5}{12} \kappa \epsilon_1^2 \xi^3 |E_g| n^2 (n^2 - 1), \quad (85)$$

which is independent of  $f$ , while for the Zeeman-type contribution one obtains

$$\langle \delta V_\theta \rangle_{\pm'}^{nP_{1/2}} = \frac{1}{6} g e \xi^2 E_g m_f, \quad (86)$$

where the value of  $m_f$  is restricted by  $-f \leq m_f \leq f$ . Also, one can further obtain that the unperturbed hyperfine energy levels are

$$E_{\text{hfs}}^{nP_{1/2}} = \frac{\Gamma_{1/2}}{n^3} [f(f+1) - 3/2], \quad (87)$$

where  $\Gamma_{1/2} = 5\Gamma_{3/2} = 9.8 \times 10^{-7}$  eV. In Fig. 6, we present the energy shifts of the  $nP_{1/2}$  line. We observe that the optical energy shift does not break the degeneracy of the  $nP_{1/2}$  line, but the Zeeman-type shift does. The values of the parameters

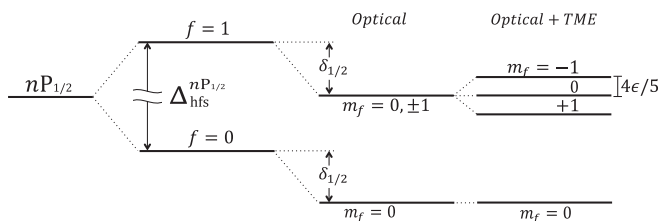


FIG. 6. Splitting of the  $nP_{1/2}$  line.

appearing in Fig. 6 are

$$\delta_{1/2} = (10/11)\delta_{3/2}, \quad \Delta_{\text{hfs}}^{nP_{1/2}} = (5/2)\Delta_{\text{hfs}}^{nP_{3/2}}, \quad (88)$$

where the parameters in the rhs are the previously defined in Eq. (84). Now we follow the same reasoning of the previous section to analyze the parameter region where our results are included. For distances of the order of  $\mu\text{m}$ , we also conclude that low values of the permittivities and low values of the quantum number  $n$  favor the Zeeman-type splitting. Thus we consider the atom to be in vacuum in front of the TI TIBiSe<sub>2</sub> and consider the energy shifts on the  $2P_{1/2}$  line. By imposing the maximum optical energy shift  $\delta_{1/2}$  to be three orders of magnitude smaller than the hyperfine splitting  $\Delta_{\text{hfs}}^{2P_{1/2}}$ , we determine  $b \sim 5511a_0 = 0.29 \mu\text{m}$ . The corresponding energies splitting become  $\delta_{1/2} = 2.43 \times 10^{-10}$  eV and  $\epsilon = 192$  Hz.

## VI. THE CASIMIR-POLDER INTERACTION IN THE $2P_j$ LINE

In this section, we examine the corrections due to the TME to the standard Casimir-Polder potential in order to determine their possible impact upon some scattering experiments designed to test the potential [33,34]. The general form of the CP potential for a hydrogen atom as a function of  $y = \xi^{-1}$  is

$$V_{\text{CP}}(y) = -|E_g| \left[ \frac{P}{y^3} + (\theta/\pi) m_f \frac{Q}{y^2} \right], \quad (89)$$

with

$$P = \frac{\epsilon_1}{8} \frac{2(\epsilon_2 - \epsilon_1) + \tilde{\theta}^2}{2(\epsilon_2 + \epsilon_1) + \tilde{\theta}^2} \langle \tilde{r}^2 \rangle_{nt} \Sigma_{Z=1}^{ijf m_f},$$

$$Q = \frac{\alpha^2}{2} \frac{g_{\text{fs}}^{(Z=1)} g_{\text{hfs}}}{2(\epsilon_2 + \epsilon_1) + \tilde{\theta}^2}, \quad (90)$$

where we have taken  $\mu_1 = \mu_2 = 1$ . Note that the value of the parameters (90) depend on the specific state under consideration. Also, we observe that  $Q \geq 0$ , while  $P \geq 0$  for  $\epsilon_2 \geq \epsilon_1$  and  $P < 0$  for  $\epsilon_2 < \epsilon_1$ . Here, we consider  $P \geq 0$ , which is the physically interesting case.

The magnetoelectric effects arise predominantly from the term proportional to  $\theta m_f Q$ , though there are also corrections in the coefficient  $P$ . For  $\theta = 0$ , Eq. (89) correctly reduces to the usual attractive CP potential between a hydrogen atom and a dielectric half-space. However, when  $\theta \neq 0$  is considered, two interesting cases appear: (i)  $\theta m_f > 0$  and (ii)  $\theta m_f < 0$ . In the first case, the full CP potential (89) retains its original attractive form in the whole range  $0 < b < \infty$ , showing only a slight decrease with respect to the usual case. The second case is in principle more interesting because now the second term in Eq. (89) is negative; therefore, the potential goes to  $-\infty$  when  $b$  approaches zero, but tends to zero, from the positive side, when  $b \rightarrow \infty$ . In fact, one can further show that the CP potential (89) has a zero at  $b_0$ , with

$$y_0 = \frac{b_0}{a_0} = |(\theta/\pi) m_f|^{-1} \frac{P}{Q}, \quad (91)$$

and a positive maximum at  $y_{\text{max}} = b_{\text{max}}/a_0 = 3y_0/2$ , given by

$$V_{\text{CP}}^{\text{max}} = |E_g| \frac{P}{2y_{\text{max}}^3}. \quad (92)$$



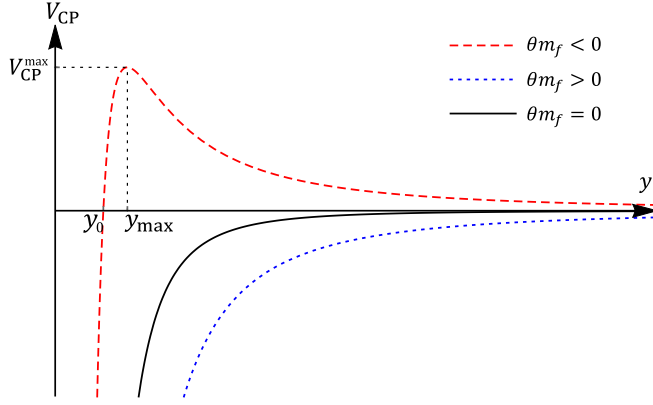


FIG. 7. Tunability between the attractive and repulsive character of the Casimir-Polder potential  $V_{CP}(y)$ .

In other words, for  $\theta m_f < 0$  the CP potential is attractive in the range  $0 < b < b_{\max}$  and repulsive when  $b_{\max} < b$ . A generic and very qualitative form of the CP potential (89) is shown in Fig. 7. These types of potentials are known in the literature as attractive potential tails and they lead to the phenomenon known as quantum reflection, which has attracted great attention in recent years from both the theoretical and experimental sides. In some applications, the repulsive contribution to the CP potential is induced by evanescent light above a glass surface; however, in our CP potential (89) the repulsive tail is generated by the interaction between the image magnetic monopoles and the atomic angular momentum. Actually, the attractive and repulsive character of the CP potential (89) can be tuned by means of the TMEP  $\theta$  for a given value of  $m_f$ , where the sign of  $\theta$  is determined by the direction of the magnetization of the coating on the surface of the TI.

Now we are interested in making some estimations regarding the position of the maximum  $b_{\max}$  and the value of the CP potential there  $V_{CP}^{\max}$ . Let us consider the nuclear charge  $Z$ , the permittivities  $\varepsilon_1$  and  $\varepsilon_2$ , and the TMEP  $\theta$  as the independent variables which we can control. Because we are working in the nonretarded approximation, we have to make sure that the range of applicability  $b$  of our estimations is such that  $b < \lambda_C$ , where  $\lambda_C$  is a wavelength characteristic of the atomic transitions to be probed and which depends crucially upon the experimental setup. The values of  $\lambda_C$  range from  $\sim 7.8 \mu\text{m}$ , when dealing with transitions in the  $n = 1, 2, 3$  sector, to values of  $\sim 7.9 \times 10^7 \mu\text{m}$  for transitions within the  $n = 2$  hyperfine sector.

A simple analysis reveals that low principal quantum numbers together with high nuclear charges favor the maximum of the CP potential. Thus, let us restrict the analysis to the maximally projected  $2P_{3/2}$  states considered in the previous section, i.e., with  $f = 2$  and  $m_f = -2$  provided  $\theta > 0$ , or alternatively, with  $m_f = +2$  and  $\theta < 0$ . In this way, from Eqs. (91) and (92) we obtain

$$y_{\max} = \frac{15\varepsilon_1}{\alpha} \frac{2(\varepsilon_2 - \varepsilon_1) + \tilde{\theta}^2}{\tilde{\theta}}, \quad (93)$$

$$V_{CP}^{\max} = \frac{|E_g| \alpha^3}{1332 \varepsilon_1^2} \frac{\tilde{\theta}^3}{[2(\varepsilon_2 + \varepsilon_1) + \tilde{\theta}^2][2(\varepsilon_2 - \varepsilon_1) + \tilde{\theta}^2]}.$$

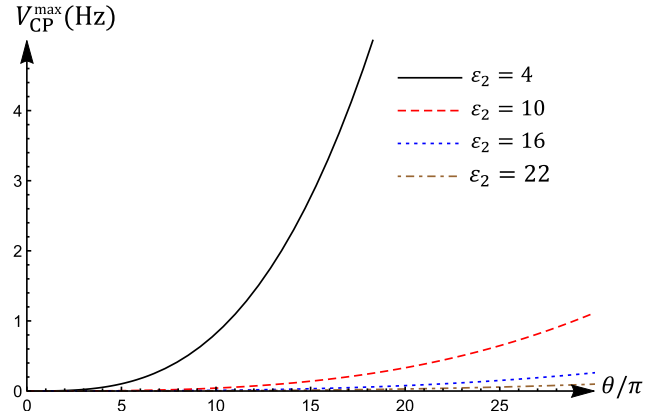
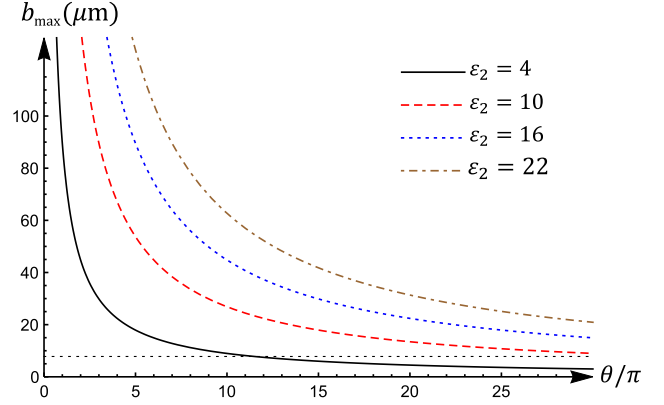


FIG. 8. Values of  $b_{\max}$  and  $V_{CP}^{\max}$  for the maximally projected  $2P_{3/2}$  state as a function of  $\theta$  for different values of  $\varepsilon_2$ .

One can further see that both  $y_{\max}$  and  $V_{CP}^{\max}$  have critical points at  $\tilde{\theta} = \sqrt{2(\varepsilon_2 - \varepsilon_1)}$  and  $\tilde{\theta} = \sqrt{-(2\varepsilon_1/3) + \sqrt{(2\varepsilon_1/3)^2 + 4(\varepsilon_2^2 - \varepsilon_1^2)}}$ , respectively. However, none of them are physically accessible provided  $\varepsilon_1 \neq \varepsilon_2$  since they require very high values of the TMEP. In the following, let us discuss the case of a hydrogen atom near the surface of the TI TlBiSe<sub>2</sub>.

In Figs. 8(a) and 8(b), we present the  $b_{\max}$  in units of  $\mu\text{m}$  and the  $V_{CP}^{\max}$  in units of Hz, corresponding to the line  $2P_{3/2}$  with  $f = 2$  and  $|m_f| = 2$ . First, we consider the situation where one is probing transitions from the  $n = 2$  to the  $n = 1$  level, where we must satisfy  $b_{\max} \ll 7.8 \mu\text{m}$ , which corresponds to the horizontal dashed line in Fig. 8(a). From the figure, we observe that this upper limit would require larger values of  $\theta$  as far as  $\varepsilon_2$  grows. As emphasized in Refs. [23] and [24], values of  $\theta \gtrsim 15\pi$  induce more general magnetoelectric couplings not included in the effective theory we are considering in Eq. (1). Thus, we take  $\theta = 15\pi$  as an upper value for this parameter. Just requiring  $b_{\max}$  to be  $7.8 \times 10^{-1} \mu\text{m}$ , for example, requires  $\varepsilon_2 = 1.43$  for  $\theta = 15\pi$ . Setting the stronger limit of  $7.8 \times 10^{-2} \mu\text{m}$  yields  $\varepsilon_2 = 1.038$ . The other limiting case is  $\theta = \pi$ , which leads to  $\varepsilon_2 = 1.029$  and  $\varepsilon_2 = 1.0029$  respectively. Notice that even the stronger limit  $b_{\max} = 7.8 \times 10^{-2} \mu\text{m} = 78 \text{ nm}$  is larger than the thickness  $w$  of the magnetic coating covering the TI surface, which is of the order of  $6 \text{ nm}$  [23]. Nevertheless, it seems rather unlikely that TIs with such small

values of  $\varepsilon_2$  are to be found. These estimations, together with the energy shifts calculated in the previous sections, reinforce the idea that one should probe beyond the hyperfine transitions. In this way, the limiting condition for the validity of the nonretarded approximation comfortably extends to  $b \ll \lambda_C \sim m$ . Because we would like a large value for  $V_{\text{CP}}^{\text{max}}$ , Fig. 8(b) suggests the choice of small value for  $\varepsilon_2$  together with a high value for  $\theta$ . Taking  $\varepsilon_2 = 4$  and  $\theta = 15\pi$  yields  $V_{\text{CP}}^{\text{max}} \sim 4.2$  Hz. Unfortunately, this value is about  $2 \times 10^{-4}$  times smaller than the optical contribution to the splitting of the  $f = 2$  level in the  $2P_{3/2}$  line which is about 21 kHz, as can be seen in Fig. 4. The corresponding location of this maximum is  $B_{\text{max}} = 5.4 \mu\text{m}$ . If we substantially increase  $V_{\text{CP}}^{\text{max}}$  to 1 kHz, just to barely include it in region of accessibility depicted in Fig. 5, we require the lower value  $\varepsilon_2 = 1.3$  with  $\theta = 15\pi$ . In this case,  $B_{\text{max}} = 0.8 \mu\text{m}$ .

## VII. DISCUSSION AND CONCLUSIONS

In conclusion, we have presented an alternative way to probe the topological magnetoelectric effect (TME) based upon high-precision spectroscopy of hydrogenlike ions, including the hydrogen atom, placed at a fixed distance from a planar topological insulator (TI), of which the surface states have been gapped by time-reversal symmetry breaking. We consider the atom to be embedded in a trivial insulator with optical properties  $(\varepsilon_1, \mu_1)$  and that the TI is characterized by the set of parameters  $(\varepsilon_2, \mu_2, \theta)$ . The coupling between the atomic electron and the image magnetic monopoles produces additional contributions to the Casimir-Polder potential while the ion-TI interaction modifies the energy shifts in the spectrum, which now became dependent on the ion-surface distance  $b$ . As expected, we find that the topological contributions are screened by the nontopological ones.

In order to suppress the trivial electrostatic effects, we considered the case in which the optical properties of the dielectric medium are comparable with that of the TI, i.e.,  $\varepsilon_1 = \varepsilon_2$  and  $\mu_1 = \mu_2 = 1$ . In this case, we find a Zeeman-type splitting of the hyperfine structure which arises directly from the coupling between the image magnetic monopole fields and the orbital and spin degrees of freedom of the atomic electron. We discussed the lowest lying energy levels where the TME effects become manifest. For hydrogenlike ions ( $Z \neq 1$ ), we find the ground state  $1S_{1/2}$  to exhibit an energy splitting  $|\langle \delta V_\theta \rangle| \sim 10$  Hz which is a factor  $10^{-6}$  smaller than the hyperfine energy level for the  $^3\text{He}^+$  ion in front of the recently discovered topological insulator TlBiSe<sub>2</sub>. We also find that circular Rydberg ions can enhance the maximal energy shifts and we determine that the maximum value for the TME correction is  $|\langle \delta V_\theta \rangle| = 1.83 \times 10^6$  Hz for the  $^{113}\text{In}^{48+}$  ion. For this improvement to be significant, one must probe transitions such that  $\Delta n \gg 1$ . We demonstrated that the case  $\varepsilon_1 \neq \varepsilon_2$  leads to a worse estimations for the maximum energy shifts.

Our analysis of the impact of the TME in circular Rydberg hydrogenlike ions has been mainly motivated by the recent proposal at NIST of boosting an experimental program for testing theory with one-electron ions in high angular momentum states

[50]. In fact, more stringent test of theory may be possible if predictions can be compared with precision frequency measurements in this regime [51,52]. As already mentioned, in the case where  $\varepsilon_1 = \varepsilon_2$ , the optical contribution can be much suppressed with respect to that of the TME, which in turn can be of the order of the hyperfine structure energy shifts. Previous measurement of the hyperfine splitting in the ground state of hydrogenlike  $^{209}\text{Bi}^{82+}$  in the optical regime was reported some time ago in Ref. [53]. Thus, having in mind the NIST proposal, one might hope that new techniques in spectroscopy might be able to incorporate higher angular momentum states and also to integrate the optical, terahertz, and radio-frequency domains [54].

Section V was devoted to the analysis of the interaction between a hydrogen atom ( $Z = 1$ ) in vacuum and the TI TlBiSe<sub>2</sub>. In this case, we find that the Zeeman-type splitting is present only in the lines with nonzero angular momentum ( $\ell \neq 0$ ) and is favored by high values of the TMEP  $\theta$ . We considered such effects on the  $2P_{3/2}$  and  $2P_{1/2}$  lines of hydrogen, obtaining the value  $b = 0.23 \mu\text{m}$  for the effect to be within the theoretical uncertainties in the corresponding parameters of the line. The parameter  $\epsilon$ , which measures the Zeeman-type energy splitting of the hyperfine structure, as shown in Figs. 4 and 6, is found to be  $\epsilon = 388$  Hz for  $\theta = \pi$ , but its value becomes  $\epsilon = 4.2$  kHz for  $\theta = 11\pi$ . We have also discovered an interesting characteristic in the Casimir-Polder potential of the  $2P_j$  lines, which is the tunability between the attractive and repulsive character of the CP interaction. We find that, for  $\theta m_f > 0$ , the CP potential retains its usual attractive form, while for  $\theta m_f < 0$  it acquires a positive maximum  $V_{\text{CPmax}}$  located at a distance  $B_{\text{max}}$ , thus implying the CP potential turns out to be repulsive for distances  $b > b_{\text{max}}$ . This is consistent with previous calculations which show that Casimir forces can be repulsive if they involve magnetic moments couplings [55,56]. In a similar fashion, it was recently shown that the dynamical properties of the atomic electron can be tuned with the TMEP  $\theta$  [57]. For the TI TlBiSe<sub>2</sub>, we obtain  $V_{\text{CPmax}} = 4.2$  Hz, which is  $10^{-2}$  smaller than the theoretical uncertainty in the splitting of the  $2P_{3/2}$  line. This maximum is located at  $b_{\text{max}} = 5.4 \mu\text{m}$ . If we substantially increase  $V_{\text{CPmax}}$  to 1 kHz, just to barely include it in region of accessibility depicted in Fig. 5, we require the rather low value  $\varepsilon = 1.3$  with  $\theta = 15\pi$ . In this case, the maximum is located at  $b_{\text{max}} = 0.8 \mu\text{m}$ . As shown in Fig. 8(b), higher values of  $V_{\text{CPmax}}$  can be obtained from low- $\varepsilon$  TIs together with high values of  $\theta$ . Nevertheless, the latter condition demands the inclusion of additional magnetoelectric effects not considered in our model.

In our work, we have assumed that the magnetic coating has no effect on the energy shifts. However, the ferromagnet makes a magnetic field which in turn will induce a Zeeman splitting, and thus it is necessary to distinguish between these two contributions in order to measure the topological contribution (63). In the present case, the magnetic field is sourced by the magnetization  $\mathbf{M} = M \hat{\mathbf{e}}_z$  of the coating, along the symmetry axis, and we can estimate it as that produced by a magnetic dipole  $\mathbf{m} = MV \hat{\mathbf{e}}_z$ , where  $V$  is the volume of the coating. For a fixed ion-surface distance, this yields to a total Zeeman energy splitting of the form

$$\epsilon(M) = aM + \text{sgn}(M) \epsilon_{\text{topo}}, \quad (94)$$

where  $a$  is a constant. The first term corresponds to the energy shifts due to the magnetic coating, while the second term corresponds to the topological contribution  $\langle \delta V_\theta \rangle$  given by Eq. (63) together with the fact that the sign of  $\theta$  is defined by the direction of the magnetization. Consequently, the topological contribution can be obtained by measuring  $\epsilon(M)$  at different magnetizations  $M$  and extracting the linear extrapolation of  $\epsilon(M)$  as  $M \rightarrow 0^+$ .

## ACKNOWLEDGMENTS

We acknowledge helpful discussions with R. Jáuregui, J. Jiménez-Mier, D. Sahagún, and A. Cortijo. We thank the referee for suggestions which have substantially improved the scope of this work. This work is supported in part by Project No. IN104815 from Dirección General Asuntos del Personal Académico (Universidad Nacional Autónoma de México) and CONACyT (México), Project No. 237503.

- [1] P. W. Anderson, *Basic Notions of Condensed Matter Physics* (Westview Press, Boulder, CO, 1997).
- [2] X.-L. Qi, T. L. Hughes, and S.-C. Zhang, *Phys. Rev. B* **78**, 195424 (2008).
- [3] S. C. Zhang, *Int. J. Mod. Phys. B* **6**, 25 (1992).
- [4] X.-L. Qi and S.-C. Zhang, *Rev. Mod. Phys.* **83**, 1057 (2011).
- [5] M. Z. Hasan and C. L. Kane, *Rev. Mod. Phys.* **82**, 3045 (2010).
- [6] C. L. Kane and E. J. Mele, *Phys. Rev. Lett.* **95**, 226801 (2005).
- [7] L. Fu and C. L. Kane, *Phys. Rev. B* **76**, 045302 (2007).
- [8] D. Hsieh, D. Qian, L. Wray, Y. Xia, Y. S. Hor, R. J. Cava, and M. Z. Hasan, *Nature (London)* **452**, 970 (2008).
- [9] H. Zhang, C.-X. Liu, X.-L. Qi, X. Dai, Z. Fang, and S.-C. Zhang, *Nat. Phys.* **5**, 438 (2009).
- [10] C.-X. Liu, X.-L. Qi, H. J. Zhang, X. Dai, Z. Fang, and S.-C. Zhang, *Phys. Rev. B* **82**, 045122 (2010).
- [11] T. Sato, K. Segawa, H. Guo, K. Sugawara, S. Souma, T. Takahashi, and Y. Ando, *Phys. Rev. Lett.* **105**, 136802 (2010).
- [12] F. Wilczek, *Phys. Rev. Lett.* **58**, 1799 (1987).
- [13] X.-L. Qi, R. Li, J. Zang, and S.-C. Zhang, *Science* **323**, 1184 (2009).
- [14] A. Karch, *Phys. Rev. Lett.* **103**, 171601 (2009).
- [15] A. Martín-Ruiz, M. Cambiaso, and L. F. Urrutia, *Phys. Rev. D* **94**, 085019 (2016).
- [16] J. Maciejko, X.-L. Qi, H. D. Drew, and S.-C. Zhang, *Phys. Rev. Lett.* **105**, 166803 (2010).
- [17] W.-K. Tse and A. H. MacDonald, *Phys. Rev. B* **82**, 161104(R) (2010).
- [18] W.-K. Tse and A. H. MacDonald, *Phys. Rev. B* **84**, 205327 (2011).
- [19] W.-K. Tse and A. H. MacDonald, *Phys. Rev. Lett.* **105**, 057401 (2010).
- [20] J. A. Crosse, S. Fuchs, and S. Y. Buhmann, *Phys. Rev. A* **92**, 063831 (2015).
- [21] J. A. Crosse, *Phys. Rev. A* **94**, 033816 (2016).
- [22] A. Martín-Ruiz, M. Cambiaso, and L. F. Urrutia, *Eur. Phys. Lett.* **113**, 60005 (2016).
- [23] A. G. Grushin and A. Cortijo, *Phys. Rev. Lett.* **106**, 020403 (2011).
- [24] A. G. Grushin, P. Rodríguez-Lopez, and A. Cortijo, *Phys. Rev. B* **84**, 045119 (2011).
- [25] V. Dziom, A. Shuvaev, A. Pimenov, G. V. Astakhov, C. Ames, K. Bendias, J. Böttcher, G. Tkachov, E. M. Hankiewicz, C. Brüne, H. Buhmann, and L. W. Molenkamp, *Nat. Commun.* **8**, 15197 (2017).
- [26] S. Y. Buhmann, *Dispersion Forces I* (Springer-Verlag, Berlin, 2012).
- [27] K. A. Milton, *The Casimir Effect: Physical Manifestation of the Zero-Point Energy* (World Scientific, Singapore, 2001).
- [28] S. Swanberg, *Atomic and Molecular Spectroscopy*, 4th ed. (Springer-Verlag, Berlin, 2004).
- [29] J. E. Lennard-Jones, *Trans. Faraday Soc.* **28**, 333 (1932).
- [30] H. B. G. Casimir and D. Polder, *Phys. Rev.* **73**, 360 (1948).
- [31] D. Raskin and P. Kush, *Phys. Rev.* **179**, 712 (1969).
- [32] A. Anderson, S. Haroche, E. A. Hinds, W. Jhe, and D. Meschede, *Phys. Rev. A* **37**, 3594 (1988).
- [33] F. Shimizu, *Phys. Rev. Lett.* **86**, 987 (2001).
- [34] H. Friedrich, G. Jacoby, and C. G. Meister, *Phys. Rev. A* **65**, 032902 (2002).
- [35] C. I. Sukenik, M. G. Boshier, D. Cho, V. Sandoghdar, and E. A. Hinds, *Phys. Rev. Lett.* **70**, 560 (1993).
- [36] V. V. Ivanov *et al.*, *J. Opt. B: Quantum Semiclass. Opt.* **6**, 454 (2004).
- [37] L. Oroszlány and A. Cortijo, *Phys. Rev. B* **86**, 195427 (2012).
- [38] A. Martín-Ruiz, M. Cambiaso, and L. F. Urrutia, *Phys. Rev. D* **92**, 125015 (2015).
- [39] A. Martín-Ruiz, M. Cambiaso, and L. F. Urrutia, *Phys. Rev. D* **93**, 045022 (2016).
- [40] C. Eberlein and R. Zietal, *Phys. Rev. A* **75**, 032516 (2007).
- [41] C. Eberlein and R. Zietal, *Phys. Rev. A* **83**, 052514 (2011).
- [42] R. de Melo e Souza, W. J. M. Kort-Kamp, C. Sigaud, and C. Farina, *Am. J. Phys.* **81**, 366 (2013).
- [43] V. M. Shabaev, *J. Phys. B: At., Mol. Opt. Phys.* **27**, 5825 (1994).
- [44] G. Barton, *Proc. R. Soc. London, Ser. A* **410**, 175 (1987).
- [45] A. E. Kramida, *At. Data Nucl. Data Tables* **96**, 586 (2010).
- [46] M. Horbatsch and E. A. Hessels, *Phys. Rev. A* **93**, 022513 (2016).
- [47] L. Chen and S. Wan, *Phys. Rev. B* **85**, 115102 (2012).
- [48] W. Nie, R. Zeng, Y. Lan, and S. Zhu, *Phys. Rev. B* **88**, 085421 (2013).
- [49] R. Zeng, L. Chen, W. Nie, M. Bi, Y. Yang, and S. Zhu, *Phys. Lett. A* **380**, 2861 (2016).
- [50] J. N. Tan, S. M. Brewer, and N. D. Guise, *Phys. Scr.* **T144**, 014009 (2011).
- [51] U. D. Jentschura, P. J. Mohr, and J. N. Tan, *J. Phys. B: At. Mol. Opt. Phys.* **43**, 074002 (2010).
- [52] U. D. Jentschura, P. J. Mohr, J. N. Tan, and B. J. Wundt, *Phys. Rev. Lett.* **100**, 160404 (2008).
- [53] I. Kluft, S. Borneis, T. Engel, B. Fricke, R. Grieser, G. Huber, T. Kuhl, D. Marx, R. Neumann, S. Schroder *et al.*, *Phys. Rev. Lett.* **73**, 2425 (1994).
- [54] A. Marian *et al.*, *Science* **306**, 2063 (2004).
- [55] B.-S. Skagerstam, P. K. Rekdal, and A. H. Vaskinn, *Phys. Rev. A* **80**, 022902 (2009).
- [56] T. H. Boyer, *Phys. Rev. A* **9**, 2078 (1974).
- [57] A. Martín-Ruiz and E. Chan-López, *Eur. Phys. Lett.* **119**, 53001 (2017).